

The optical depth of the Universe for ultra-high energy cosmic ray scattering in the magnetized large scale structure

Kumiko Kotera* and Martin Lemoine†
Institut d'Astrophysique de Paris
UMR7095 - CNRS, Université Pierre & Marie Curie,
98 bis boulevard Arago
F-75014 Paris, France
 (Dated: June 21, 2024)

This paper provides an analytical description of the transport of ultra-high energy cosmic rays in an inhomogeneously magnetized intergalactic medium. This latter is modeled as a collection of magnetized scattering centers such as radio cocoons, magnetized galactic winds, clusters or magnetized filaments of large scale structure, with negligible magnetic fields in between. Magnetic deflection is no longer a continuous process, it is rather dominated by scattering events. We study the interaction between high energy cosmic rays and the scattering agents. We then compute the optical depth of the Universe to cosmic ray scattering and discuss the phenomenological consequences for various source scenarios. For typical parameters of the scattering centers, the optical depth is greater than unity at 5×10^{19} eV, but the total angular deflection is smaller than unity. One important consequence of this scenario is the possibility that the last scattering center encountered by a cosmic ray be mistaken with the source of this cosmic ray. In particular, we suggest that at least part of the correlation recently reported by the Pierre Auger Observatory may be affected by such delusion: this experiment may be observing the last scattering surface of ultra-high energy cosmic rays rather than their source population. Since the optical depth falls rapidly with increasing energy, one should probe the arrival directions of the highest energy events beyond 10^{20} eV on an event by event basis to circumvent this effect.

PACS numbers: Valid PACS appear here

I. INTRODUCTION

The problem of the origin of ultra-high energy cosmic rays has generally been expressed as the conjunction of two questions: *(i)* how can particles be accelerated to energies in excess of 10^{20} eV? *(ii)* why is the source not seen in the arrival directions of the highest energy events? Progress on the former question has certainly been hindered by our relative lack of knowledge on acceleration mechanisms and high energy processes in the most powerful astrophysical objects. Regarding the latter question, progress has been mostly limited by the scarcity of experimental data at the highest energies, at least until very recently.

Indeed the first results of the Pierre Auger Observatory, which have just been published, report a significant correlation of the arrival directions of the highest energy events with a catalog of active galactic nuclei (AGN) closer than 75 Mpc [1, 2]. This observation certainly marks an important step in the search for the source of ultra-high cosmic rays. However one should not over-interpret the significance of these results. In particular, the likelihood of the reported coincidence rests on the comparison with isotropic arrival directions, yet the large scale structure is known to be highly inhomogeneous at least up to 75 Mpc. Since AGN are known to

cluster with the large scale structure, one cannot exclude at present that the observed correlation remains a coincidence if the source itself clusters with the large scale structure [2]. More will be said on these data in Section IV of the present paper.

Furthermore, there exist other (and sometimes contradictory) claims in the literature on the existence of correlations of ultra-high energy cosmic ray arrival directions with various source catalogs [3], the strongest being the association with BL Lacertae objects reported in Refs. [4, 5, 6] (see also Refs. [7, 8]). Since the existing data is so scarce at the highest energies, the assessment of the statistical significance remains a difficult task. Finally, the reported evidence for multiplets of events tends to suggest that the source lies in the arrival direction of the events clusters. However some of these clusters show interacting galaxies as the sole peculiar objects on the line of sight [9], while a more recent multiplet appears correlated with interacting clusters of galaxies [10, 11]. Taken at face value, all these claims do not allow to draw a clear and consistent picture of the source of ultra-high energy cosmic rays.

It is admitted that cosmic magnetic fields must play a key role in this puzzle, although which role exactly is also a question that is still seeking for an answer. And this source of uncertainty is in turn related to our poor knowledge of the strength and the distribution of extragalactic magnetic fields (see Ref. [12, 13] for detailed reviews of existing data). There exists a rather large body of literature on the relation between cosmic magnetic fields and ultra-high energy cosmic rays. Most recent studies

*Electronic address: kotera@iap.fr

†Electronic address: lemoine@iap.fr

have constructed models of extra-galactic magnetic fields and then resorted to Monte Carlo simulations in order to quantify the influence of these fields on the time, energy and angular images expected in large scale detectors. In general, the magnetic field is assumed to be all pervading, with some degree of inhomogeneity, in which case magnetic deflection is a continuous process.

However, if one attributes the origin of the extragalactic magnetic field to pollution by a sub-class of galaxies, for instance starburst galaxies [14, 15, 16] or radio-galaxies [17, 18, 19], one should expect a high degree of inhomogeneity, directly related to the hierarchical clustering of matter in the Universe. Even if the magnetic field is produced in a somewhat more uniform matter at high redshift (see Ref. [20] for a review of models of the origin of large scale magnetic fields), then the present-day magnetic field should be highly inhomogeneous, as a result of the amplification of the magnetic field in the shear and compressive flows associated with the formation of non-linear structures [21, 22, 23, 24] (see also [25] for a general discussion). In these simulations, voids in the large scale structure are essentially deprived of magnetic field.

In the present paper we propose an analytical description of the transport of ultra-high energy cosmic rays in an inhomogeneous medium composed of scattering centers in an essentially unmagnetized intergalactic medium. These scattering centers comprise the filaments just as the clusters of galaxies but also all possible regions of locally enhanced magnetic fields, such as galactic winds, groups of galaxies, large scale structure shocks and fossil radio-galaxy cocoons.

The present study is further motivated by the fact that Refs. [21, 22, 23, 24] diverge as to the conclusions they draw on the influence of the extra-galactic magnetic fields on ultra-high energy cosmic rays, even though they try to construct ab initio predictions for the distribution of these large scale magnetic fields. This difference stems from the uncertainty on the origin of these magnetic fields, not withstanding the complexity of modeling accurately the evolution of magnetic fields in the formation of large scale structure. Such a situation then calls for new tools to model and understand the propagation of high energy cosmic rays in inhomogeneous cosmic magnetic fields.

In the present description, magnetic deflection is no longer a continuous process, but is instead dominated by scattering events. We thus introduce the notion of the optical depth of the Universe to ultra-high energy cosmic ray scattering and discuss the phenomenological consequences. In particular, we show that the optical depth decreases very abruptly as the energy increases, because the source distance scale decreases due to increasing energy losses, and because the influence of cosmic magnetic fields diminishes with increasing energy.

We argue that the energy beyond which the Universe becomes semi-transparent or transparent may be tantalizingly close to the threshold beyond which experiments

search for counterparts, $E \simeq 4 - 6 \times 10^{19}$ eV. This could have profound consequences for our interpretation of existing data. For instance, if most sources lie beyond the last scattering surface, one could mistake the scattering centers on the last scattering surface (such as starbursts, old radio-galaxies or giant shock waves) with the source of ultra-high energy cosmic rays.

The phenomenological consequences thus differ widely from the case of continuous deflection in an all-pervading medium. We thus discuss in some detail the expected effects and their relation to current and future observations of cosmic ray arrival directions.

This paper is laid out as follows. In Section II, we sketch a census of possible scattering centers and their influence on the optical depth of the Universe to cosmic ray scattering. We also calculate the distance to the last scattering surface and compare it to the expected source distance scale. In Section III, we discuss the transport of cosmic rays in this strongly inhomogeneous medium and the expected observational consequences. Finally, in Section IV, we summarize our findings and comment on the existing data in the framework of the present model. The physics of the interaction of cosmic rays with scattering centers is discussed in Appendix A.

II. THE OPTICAL DEPTH OF THE UNIVERSE TO HIGH ENERGY COSMIC RAY SCATTERING

A. Scattering centers in the large scale structure

We adopt a description in which the extragalactic magnetic field is inhomogeneous. If this magnetic field originates from a sub-class of galaxies, its configuration is bound to follow that of the large scale structure since the mixing length in the Universe is small for cosmological standards: for typical intergalactic velocities of ~ 300 km/s, the length traveled in a Hubble time is only $\simeq 4$ Mpc.

Obviously, at a given energy, the total optical depth to cosmic ray scattering is dominated by the structures with the largest $n\sigma$, where n represents the space density and σ the cross-section of the magnetized halo. One should thus focus on the radio halos of radio-galaxies, the magnetized winds of star forming galaxies, and on larger scales to clusters of galaxies and filaments as well as their surrounding accretion shock waves.

1. Radio halos

Radio halos of old radio-galaxies (deemed radio ghosts) have been already considered as possible sites of ultra-high energy cosmic ray scattering in Ref. [26]. This study evaluates their space density as $n_{\text{rg}} \simeq 10^{-2} - 10^{-1} \text{ Mpc}^{-3}$, the size of their magnetized halos as $r_{\text{rg}} \sim 0.5 - 1 \text{ Mpc}$ and their magnetic field $B_{\text{rg}} \sim 1 \mu\text{G}$. Such quasar outflows have also been examined in detail in

Ref. [18] as a site of magnetic pollution of the intergalactic medium, but their results differ from those above. These latter authors find a much lower magnetic field strength $B_{\text{rg}} \sim 10^{-9}$ G, and a substantially larger extent, $r_{\text{rg}} \simeq 1 - 5$ Mpc, for a comparable space density. With respect to the results of Ref. [18], the scattering should be dominated by the sub-population of recently formed quasars (at redshifts $z \lesssim 4$), which have $r_{\text{rg}} \sim 2 - 4$ Mpc and $B_{\text{rg}} \sim 3 \times 10^{-9}$ G. The main difference between these calculations results from the different modeling of the bubble evolution. The former study assumes that the bubble settles in pressure equilibrium in a rather dense and hot intergalactic environment (with $\rho/\langle\rho\rangle \sim 30$ and $T \simeq 10^8$ K) while the latter argues that the bubble expands until its velocity matches that of the Hubble flow and takes the surrounding IGM to be much colder and less dense ($T \sim 10^4$ K and $\rho/\langle\rho\rangle = 1$). Both fix the magnetic strength to lie at a fraction of equipartition with thermal energy, although this fraction to equipartition $\epsilon_B = 0.5$ in Ref. [26] and $\epsilon_B = 0.1$ in Ref. [18]; furthermore, Ref. [18] adopt ϵ_B as the equipartition fraction before expansion of the bubble, assuming that the magnetic field then decays with expansion. This study thus neglects all possible further amplification mechanisms of B , hence their estimate (at a given ϵ_B) should be considered as a lower limit. If one instead considers ϵ_B as the equipartition fraction of the magnetic field at present, the magnetic field strength inside the bubble can be related to the kinetic energy of the outflow and the size of the bubble as follows:

$$B_{\text{rg}} = 5 \times 10^{-8} \text{ G} \left(\frac{\epsilon_B}{0.1} \right)^{1/2} \left(\frac{E_{\text{rg}}}{10^{59} \text{ ergs}} \right)^{1/2} \left(\frac{R_{\text{rg}}}{1 \text{ Mpc}} \right)^{-3/2} \quad (1)$$

This latter estimate agrees with the conclusions of Ref. [19] which studies the degree of magnetization of the IGM by radio-galaxies jets and lobes. The outflow energy 10^{59} ergs is an average energy for a quasar population [26]: it corresponds to a black hole mass $M_{\text{BH}} \simeq 3 \times 10^7 M_{\odot}$, radiating $L_{\text{bol}} \simeq 3 \times 10^{45}$ ergs/s over 10^7 yrs [18]. Note however that the observational compilation of Ref. [27] leads to slightly higher values for E_{rg} and B_{rg} . These authors have observed that the lobes of 70% of field radio-galaxies in their sample have a much higher energy content $\sim 10^{60} - 10^{61}$ ergs than the remaining 30% in clusters (about 10^{58} ergs), with a typical volume $V \sim 0.03 - 0.3 \text{ Mpc}^3$ and inferred minimum energy magnetic field strengths in the range $3 - 30 \mu\text{G}$. If the magnetic field is to decay as $V^{2/3}$ during the subsequent expansion of these bubbles, the final value for B_{rg} would be of order $0.1 \mu\text{G}$ for a typical radius $r_{\text{rg}} \simeq 3$ Mpc as above. In the following, we thus consider the possible range of values $B_{\text{rg}} = 1 - 10 \times 10^{-8}$ G and typical size $r_{\text{rg}} \simeq 1 - 3$ Mpc.

Finally, Refs. [18, 26] estimate the space density of quasar outflows from the observed density of quasars at high redshifts and the typical duration of the quasar phase (taken as 10^7 yrs). Their estimate of $\sim 10^{-2} -$

10^{-1} Mpc^{-3} agrees with the recent determinations of the black hole number density at low redshifts, in particular $n(> 10^7 M_{\odot}) \simeq 2 - 4 \times 10^{-2} \text{ Mpc}^{-3}$ [28]. In the following, we use $n_{\text{rg}} = 1 - 3 \times 10^{-2} \text{ Mpc}^{-3}$.

2. Magnetized galactic winds

Galactic winds have been proposed as a source of magnetic pollution of the intergalactic medium by various authors, see in particular [14, 15, 16]. Such outflows have been observed in different galaxies, for instance in the starbursting nearby dwarf galaxy M82 with wind speed $v \simeq 2000$ km/s and extension ~ 10 kpc [29], or in massive star forming Lyman break galaxies at high redshifts with wind speed $v \sim 1000$ km/s and extending as far as hundreds of kpc [30], maybe up to $\simeq 1$ Mpc [31] (see Ref. [32] for a review).

Galactic winds are also a key ingredient for theoretical models which attempt at explaining the metal enrichment of the intergalactic medium [33, 34, 35, 36]. At the present time, it is not clear which galaxy type (if any) dominates the pollution. Starburst dwarf galaxies appear more akin at producing large winds, however they also have a smaller gaseous content and a smaller energetic reservoir. In the following, we use the most recent simulations of Ref. [35] which detail the properties of galactic winds. This study shows that the number of wind-blowing galaxies is relatively insensitive to the stellar mass of the parent galaxy in the range $10^8 M_{\odot} \lesssim M_* \lesssim 10^{10} M_{\odot}$ as a result of the opposed influences of wind ram pressure and amount of infalling material, and that this number falls at both ends of this mass range. At $z \simeq 0$ and in this mass range, the typical wind radius increases slowly with galaxy mass as follows: $r_{\text{gw}} \simeq 200$ kpc for $M_* = 10^8 M_{\odot}$, $r_{\text{gw}} \simeq 800$ kpc for $M_* = 10^9 M_{\odot}$, and $r_{\text{gw}} \simeq 1$ Mpc for $M_* = 10^{10} M_{\odot}$. Overall, the contribution $n_{\text{gw}} r_{\text{gw}}^2$ will be dominated by dwarf galaxies of stellar mass $M_* \sim 10^9 M_{\odot}$. The number density n_{gw} of galaxies surrounded by a wind at $z = 0$ can be derived from the filling factor f_{gw} of the winds; unfortunately, this quantity appears to depend strongly on the model, taking values between 2×10^{-2} and unity. The median value corresponds to $f_{\text{gw}} = 0.1 - 0.2$, which gives a density $n_{\text{gw}} \simeq f_{\text{gw}}/V_{\text{gw}} \simeq 2 - 5 \times 10^{-2} \text{ Mpc}^{-3}$, with $V_{\text{gw}} = (4\pi/3)r_{\text{gw}}^3$ the wind volume. Note that this number is comparable to the number density of galaxies of stellar mass above $10^8 - 10^9 M_{\odot}$. If the filling factor becomes substantially larger, the galactic winds will overfill the filaments in which they reside, hence the filaments themselves become the scattering centers.

Concerning the strength of B_{gw} , Ref. [16] indicates that most winds have a magnetic field with $B_{\text{gw}} \simeq 10^{-8} - 10^{-7}$ G at $z = 0$, the range covering conservative and optimistic assumptions concerning the amplification of B_{gw} . Such amplification may have been detected in the outflow of M82, where a magnetic field strength as high as $10 \mu\text{G}$ [37] has been reported in the first 10 kpc.

Ref. [15] has argued that the magnetic field could be amplified through the Kelvin-Helmholtz instability during ejection.

3. Clusters of galaxies

Clusters of galaxies are rare structures in the Universe, $n_{\text{cg}} \simeq 10^{-5} h_{70}^3 \text{Mpc}^{-3}$, but they are known to host strong magnetic fields, with $B_{\text{cg|c}} \sim 1 - 10 \mu\text{G}$ in the innermost $r_{\text{cg|c}} \sim 100 \text{kpc}$ [12]. Measurements of the magnetic field in the cluster outskirts are rather scarce as a result of the smaller electron density and magnetic field strength. The minimum energy interpretation of recent synchrotron data nevertheless indicates that $B_{\text{cg}} \sim 1 \mu\text{G}$ out to $r_{\text{cg}} \sim 1 \text{Mpc}$ [38]. Theoretical expectations tend to differ. For instance, Ref. [22] shows that B varies with cluster mass, and indicates that for a massive cluster $B_{\text{cg}} \sim 1 \mu\text{G}$ within $r_{\text{cg}} \simeq 0.2 \text{Mpc}$, then falls to $B_{\text{cg}} \sim 10^{-7} \mu\text{G}$ within $r_{\text{cg}} \simeq 1 \text{Mpc}$, $B_{\text{cg}} \sim 10^{-8} \text{G}$ within $r_{\text{cg}} \simeq 2 \text{Mpc}$ and finally $B_{\text{cg}} \sim 10^{-9} \text{G}$ within $r_{\text{cg}} \simeq 4 - 5 \text{Mpc}$, while Fig.5 of Ref. [39] indicates more extended magnetic fields, with $B_{\text{cg}} \sim 1 \mu\text{G}$ within $r_{\text{cg}} \simeq 1 \text{Mpc}$, then falls to $B_{\text{cg}} \sim 10^{-7} \mu\text{G}$ within $r_{\text{cg}} \simeq 3 \text{Mpc}$, $B_{\text{cg}} \sim 10^{-8} \text{G}$ within $r_{\text{cg}} \simeq 4 \text{Mpc}$ and finally $B_{\text{cg}} \sim 10^{-9} \text{G}$ within $r_{\text{cg}} \simeq 5 \text{Mpc}$. In the following, we take these two limits as a range for B_{cg} and r_{cg} .

Note that about half of galaxies lie outside of clusters, hence one can treat clusters of galaxies and the above field radio ghosts and field galactic winds as distinct scattering centers.

4. Filaments and walls of large scale structure

Filaments or walls of large scale structure are not expected to be sources of magnetic pollution per se. However they may be pervaded with an average magnetic field produced in the accretion shocks surrounding them or generated in and ejected by the galaxies they contain, provided the filling factor of the resulting magnetic pollution in the filament/wall volume is of order unity. In the following, we will consider both possibilities.

If, as before, the magnetic energy density in the filament/wall is a fraction ϵ_B of the thermal energy of the IGM, one infers a magnetic field strength:

$$B_{\text{f}} = 3.5 \times 10^{-8} \text{G} \left(\frac{\epsilon_B}{0.1} \right)^{1/2} \left(\frac{\rho_{\text{f}}}{10 \langle \rho_{\text{b}} \rangle} \right)^{1/2} \left(\frac{T_{\text{f}}}{10^6 \text{K}} \right)^{1/2}, \quad (2)$$

ρ_{f} and T_{f} denoting the filament baryonic density and temperature.

The typical length scale of a filament is $l_{\text{f}} \sim 15 \text{Mpc}$, its radius $r_{\text{f}} \sim 1 - 2 \text{Mpc}$, and the typical separation between two filaments $d_{\text{f}} \sim 25 \text{Mpc}$ [40].

During the formation of non-linear structures, shock waves develop as a consequence of the infall of material

on filaments, walls and clusters of galaxies. Numerical simulations indicate that the typical radius of external shock waves around filament it is of the order of $r_{\text{sh}} \simeq 2 - 3 \text{Mpc}$ [41, 42]; the typical velocity of these shock waves is of order $v_{\text{sh}} \sim 300 - 1000 \text{km/s}$. Such shock waves have been proposed a site of magnetic field amplification (see for instance [43]) and cosmic ray acceleration [44, 45, 46].

If the magnetic field in the shock wave vicinity corresponds to a fraction of equipartition with the shock energy density ρv_{sh}^2 , one finds:

$$B_{\text{sh}} \simeq 10^{-7} \text{G} \left(\frac{\epsilon_B}{0.1} \right)^{1/2} \left(\frac{\rho_{\text{ext}}}{\langle \rho_{\text{b}} \rangle} \right)^{1/2} \left(\frac{v_{\text{sh}}}{1000 \text{km/s}} \right)^{1/2}. \quad (3)$$

Note that ρ_{ext} refers to the density of infalling material. The estimate $\epsilon_B \sim 0.1$ gives the right order of magnitude for the inferred value of magnetic field strength $\sim 100 \mu\text{G}$ in young supernovae remnants assuming a typical interstellar medium density and comparable shock speed [47, 48].

If cosmic shock waves amplify the magnetic field up to the value B_{sh} given above, one should then expect the filament to be endowed with a significant fraction of B_{sh} out to the shock radius. In effect, the amount of matter accreted through the shock in a Hubble time in units of the quantity of matter contained inside the structure at the present time can be expressed as:

$$f_{\text{acc}} \simeq \frac{\rho_{\text{ext}} v_{\text{sh}} H_0^{-1}}{\rho_{\text{in}} r_{\text{f}}} \sim 0.3 \left(\frac{v_{\text{sh}}}{1000 \text{km/s}} \right) \left(\frac{r_{\text{f}}}{2 \text{Mpc}} \right)^{-1} \left(\frac{\rho_{\text{f}}}{10 \langle \rho_{\text{b}} \rangle} \right)^{-1} \quad (4)$$

Note that the estimate B_{f} given in Eq. (2) agrees with that of B_{sh} to within a factor of a few (even though it was derived through other means).

B. Optical depth and last scattering surface for cosmic ray scattering

Depending on the strength of the magnetic field in a halo and its coherence length, the interaction of a particle may either lead to diffusion inside the structure, at sufficiently low energy, or to a weak deflection angle, at higher energies. The details of the interaction between a particle and a magnetized structure is described in detail in Appendix A.

1. Homogeneously distributed scattering centers

Out of simplicity, we first assume that the scattering centers are distributed homogeneously in the Universe with a typical mean free path to interaction d_i , where i refers to the type of scattering center (e.g. magnetized galactic wind, radio halo, ...). We will discuss in

Section II C the influence of inhomogeneity on the conclusions of the discussion that follows. For scattering centers of density n_i and cross-section σ_i , $d_i = (n_i\sigma_i)^{-1}$. The mean free path to interaction with any scattering center is written \bar{d} :

$$\bar{d} = \frac{1}{\sum_i n_i\sigma_i}. \quad (5)$$

The optical depth to ultra-high energy cosmic ray scattering over a path length l is then defined as:

$$\tau = \frac{l}{\bar{d}} = l \sum_i n_i\sigma_i. \quad (6)$$

The above optical depth characterizes the number of scatterings along a path length l but does not provide information on the angular spread of the cosmic ray image on the detector. Hence it is useful to introduce an effective optical depth τ_{eff} , which becomes unity when the path length l is such that the particle has suffered a deflection of order unity. If at each scattering, the squared deflection is noted $\delta\theta_i^2$, then the number of scatterings to achieve a deflection of order unity reads $1/\delta\theta_i^2$. The scattering length l_{scatt} of cosmic rays in the medium, which corresponds to the distance over which the deflection becomes of order unity, can be written as:

$$l_{\text{scatt}} = \frac{1}{\sum_i n_i\sigma_i\delta\theta_i^2}. \quad (7)$$

We thus define the effective optical depth τ_{eff} as:

$$\tau_{\text{eff}} = \frac{l}{l_{\text{scatt}}} = l \sum_i n_i\sigma_i\delta\theta_i^2. \quad (8)$$

The angular deflection can be expressed in a simple way as a function of the Larmor radius $r_{L|i}$ of the particle in structure i , of the magnetic field coherence length λ_i of this structure, and of the extent r_i . Using the formula provided in Appendix A [in particular Eq. (A3)], one can rewrite the effective optical depth as:

$$\tau_{\text{eff}} \simeq l \sum_i n_i\sigma_i \left(1 + \frac{r_{L|i}^2}{r_i\lambda_i}\right)^{-1}. \quad (9)$$

Obviously, one always has $\tau_{\text{eff}} < \tau$. One should interpret the two optical depths as follows: $\tau < 1$ (which implies $\tau_{\text{eff}} < 1$) means that the Universe is transparent to cosmic ray scattering on the scale l , while $\tau > \tau_{\text{eff}} > 1$ means that the Universe is opaque over this scale, i.e. the accumulated angular deflection is greater than unity. The intermediate regime, $\tau > 1 > \tau_{\text{eff}}$ is interesting; it corresponds to a semi-transparent situation in which cosmic rays suffer one to many scatterings but the accumulated angular deflection remains smaller than unity.

The phenomenology of the cosmic ray signal on the detector then depends on the typical source distance, which should be used for l , as well as on the characteristics of

the scattering agents described above. Assuming rectilinear propagation of the particles, the source distance scale is of order l_{max} , the maximal distance that a particle of energy E can travel without losing its energy. Indeed, if the source population is continuously emitting and homogeneous (the latter being a good approximation on scales $l \gtrsim 100$ Mpc), the flux $F(< l)$ received from sources located within a distance l increases as l :

$$F(< l) = n_s \dot{N}_{\text{UHECR}} l, \quad (10)$$

where n_s denotes the source density and \dot{N}_{UHECR} the number of cosmic rays emitted by a source per unit time. In the case of bursting sources, one finds the same scaling (see Ref. [49]):

$$F(< l) = \dot{n}_s N_{\text{UHECR}} l. \quad (11)$$

In this equation, \dot{n}_s should now be understood as the rate of bursting sources per unit time and unit volume, and N_{UHECR} as the total number of cosmic rays emitted by a source.

Hence in both cases, most of the flux comes from sources located at distance of order l_{max} . In the following, we therefore substitute l_{max} for l in the expression of the optical depth. We will discuss apart the particular case of rare close-by sources. One can evaluate the distance l_{max} in two ways: either as the energy loss distance $E |dE/dx|^{-1}$, or as the maximal distance that a particle can travel, assuming it has been detected with energy E and the maximal energy at the source is E_{max} . In the following, we use this latter definition and assume $E_{\text{max}} = 4 \times 10^{20}$ eV. The two definitions give values that never differ by more than 40% however, over the energy range 10^{17} eV \rightarrow 10^{20} eV.

If particles diffuse rather than travel rectilinearly, the maximum distance is instead determined by $\sqrt{2Dt_{\text{max}}}$, where D denotes the diffusion coefficient and $t_{\text{max}} = l_{\text{max}}/c$. This will be discussed in more detail in Section III C 2.

We may now plot the optical depths τ and τ_{eff} as functions of energy. In Fig. 1, we show an example that ignores all scattering centers except magnetized galactic winds, for which we assume $n_{\text{gw}} = 2 \cdot 10^{-2}$ Mpc $^{-3}$, $r_{\text{gw}} = 0.8$ Mpc, $B_{\text{gw}} = 3 \cdot 10^{-8}$ G and $\lambda_{\text{gw}} = 0.05$ Mpc. The resulting optical depth τ is shown as the dashed (blue) line, and the effective optical depth τ_{eff} as the solid (red) line. The dependence of τ on E actually reveals the dependence of l_{max} on E : l_{max} decreases sharply beyond a few 10^{19} eV as a consequence of pion production on the microwave background. The dependence of τ_{eff} on E is even more pronounced, since the number of scatterings to achieve deflection of order unity rapidly increases with energy, roughly as E^2 beyond 10^{18} eV here [see Eq. (9)]. The horizontal dotted line indicates an optical depth of order unity, while the vertical dotted lines indicate at which energy $\tau_{\text{eff}} = 1$ and $\tau = 1$ respectively, from left to right. As indicated on the figure, these lines delimit the energy ranges in which the Universe ap-

pears opaque, semi-transparent or transparent to cosmic rays. Interestingly, for this example, the Universe is semi-transparent at energies close to the GZK cut-off threshold for pion production $E_{\text{GZK}} \simeq 6 \cdot 10^{19}$ eV [50, 51].

In Figure 2, we show the optical depths for the various types of scattering centers, taken in turn, and for two sets of parameters defining their characteristics, as indicated in the caption. In principle, one should of course sum the different optical depths of the types of scattering centers. If, however, the pollution of magnetized winds and radio halos permeate the filaments and nothing else, one should of course only consider the filaments as the sole scattering agents. The upper left panel of Fig. 2 represents the optical depth over l_{loss} assuming only radio halos. The upper right panel shows τ for magnetized galactic winds, also with different sets of parameters as before, while the lower left panel of Fig. 2 shows the optical depth for clusters of galaxies, and the lower right panel the optical depth for magnetized filaments of large scale structure.

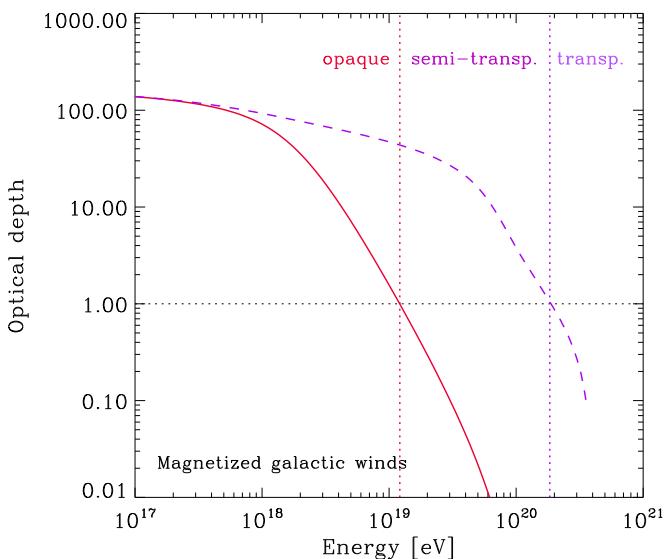


FIG. 1: Optical depth to cosmic ray scattering by magnetized galactic winds, with $n_{\text{gw}} = 2 \cdot 10^{-2} \text{Mpc}^{-3}$, $B_{\text{gw}} = 3 \cdot 10^{-8} \text{G}$, $\lambda_{\text{gw}} = 50 \text{kpc}$, and $r_{\text{gw}} = 0.8 \text{Mpc}$. Solid line: optical depth τ_{eff} to scattering by an angle of order unity, as defined in Eq. (9); dashed line: optical depth τ as defined in Eq. (6). In the energy range where $\tau > \tau_{\text{eff}} > 1$, the Universe is opaque up to the energy loss distance; in the range where $\tau > 1 > \tau_{\text{eff}}$, the Universe is semi-transparent on this distance scale, meaning that cosmic rays suffer several to many scatterings but the total angular deflection remains below unity; finally, at energies where $1 > \tau > \tau_{\text{eff}}$, the Universe is transparent to cosmic ray scattering.

The two quantities l_{scatt} and \bar{d} are shown together with the maximal path length (or source distance scale) l_{max} in Fig. 3 for magnetized galactic winds as scattering agents, with the same parameters used to construct Fig. 1. Figure 3 illustrates in a different way the opaque, semi-transparent or transparent nature of the Universe to cosmic ray scattering.

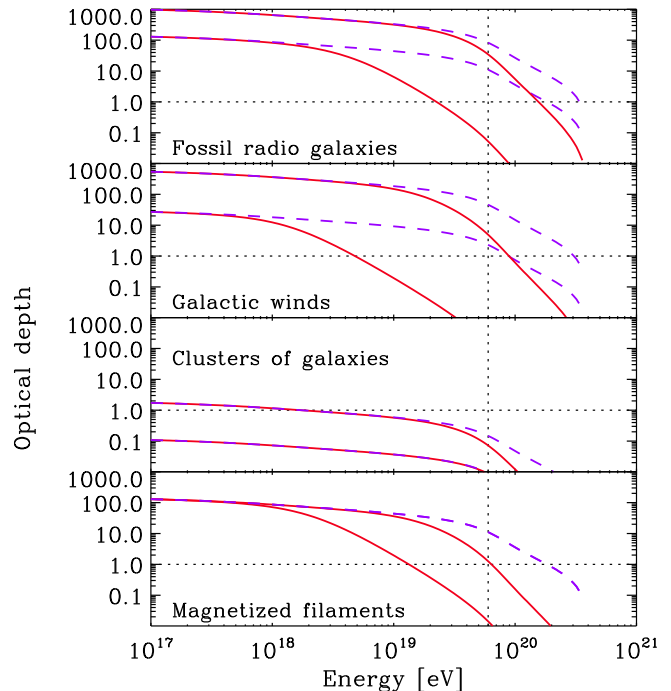


FIG. 2: Optical depth to cosmic ray scattering for different types of scattering agents and for two different sets of parameters in each case. Solid lines: optical depth τ_{eff} to scattering by an angle of order unity, as defined in Eq. (9); dashed lines: optical depth τ as defined in Eq. (6). The vertical dotted line indicates $E = 6 \times 10^{19}$ eV. Fossil radio galaxies: $n_{\text{rg}} = 3 \cdot 10^{-3} \text{Mpc}^{-3}$, $B_{\text{rg}} = 10^{-8} \text{G}$, $\lambda_{\text{rg}} = 100 \text{kpc}$, and $r_{\text{rg}} = 2 \text{Mpc}$ (lower curves); $n_{\text{rg}} = 10^{-2} \text{Mpc}^{-3}$, $B_{\text{rg}} = 10^{-7} \text{G}$, $\lambda_{\text{rg}} = 100 \text{kpc}$, and $r_{\text{rg}} = 3 \text{Mpc}$ (upper curves). Magnetized galactic winds: $n_{\text{gw}} = 10^{-2} \text{Mpc}^{-3}$, $B_{\text{gw}} = 10^{-8} \text{G}$, $\lambda_{\text{gw}} = 50 \text{kpc}$, and $r_{\text{gw}} = 0.5 \text{Mpc}$ (lower curves); $n_{\text{gw}} = 5 \cdot 10^{-2} \text{Mpc}^{-3}$, $B_{\text{gw}} = 10^{-7} \text{G}$, $\lambda_{\text{gw}} = 50 \text{kpc}$, and $r_{\text{gw}} = 0.8 \text{Mpc}$ (upper curves). Clusters of galaxies: $n_{\text{cg}} = 10^{-5} \text{Mpc}^{-3}$, $B_{\text{cg}} = 10^{-6} \text{G}$, $\lambda_{\text{cg}} = 100 \text{kpc}$, and $r_{\text{cg}} = 1 \text{Mpc}$ (lower curves); $n_{\text{cg}} = 10^{-5} \text{Mpc}^{-3}$, $B_{\text{cg}} = 10^{-7} \text{G}$, $\lambda_{\text{cg}} = 100 \text{kpc}$, and $r_{\text{cg}} = 4 \text{Mpc}$ (upper curves). Magnetized filaments of large scale structure: interseparation $d_f = 25 \text{Mpc}$, $B_f = 3 \cdot 10^{-9} \text{G}$, $\lambda_f = 300 \text{kpc}$, and $r_f = 2 \text{Mpc}$ (lower curves); $d_f = 25 \text{Mpc}$, $B_f = 3 \cdot 10^{-8} \text{G}$, $\lambda_f = 300 \text{kpc}$, and $r_f = 2 \text{Mpc}$ (upper curves).

One may also draw the analog of Fig. 2 for the distance to the last scattering surface \bar{d} for the different types of scattering centers, as done in Fig. 4.

C. Inhomogeneity of the large scale structure - Analytic discussion

The above results should be corrected for the presence of inhomogeneity when the distances considered are smaller than the inhomogeneity length 100Mpc . In a first approach, one may assume that all scattering centers are clustered in the filaments of large scale structure. This affects the transport in two ways: the typical dis-

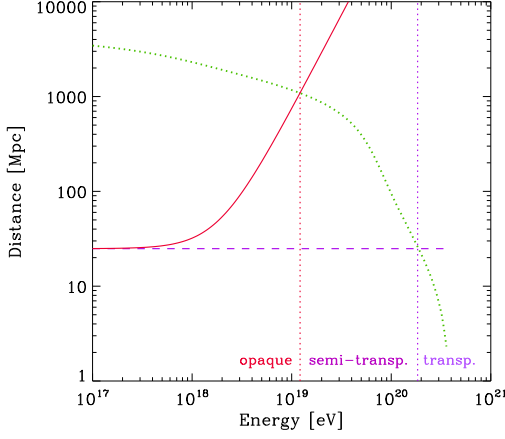


FIG. 3: Distance to the last scattering surface by magnetized galactic winds, with $n_{\text{gw}} = 2 \cdot 10^{-2} \text{ Mpc}^{-3}$, $B_{\text{gw}} = 3 \cdot 10^{-8} \text{ G}$, $\lambda_{\text{gw}} = 50 \text{ kpc}$, and $r_{\text{gw}} = 0.8 \text{ Mpc}$ as in Fig. 1. Solid line: scattering length l_{scatt} for a deflection of order unity, as defined in Eq. (7); dashed line: distance \bar{d} to the last scattering surface as defined in Eq. (5). The dotted (green) line indicates the maximal distance to the source l_{max} , which also gives the source scale. In the energy range where $\bar{d} < l_{\text{scatt}} < l_{\text{max}}$, the Universe is opaque; in the range where $\bar{d} < l_{\text{max}} < l_{\text{scatt}}$, the Universe is semi-transparent on the distance scale l_{max} , meaning that cosmic rays suffer several to many scatterings but the total angular deflection remains below unity; finally, at energies where $l_{\text{max}} < \bar{d} < l_{\text{scatt}}$, the Universe is transparent to cosmic ray scattering.

tance to an interaction becomes of order d_f rather than d_i , but the typical deflection may be enhanced, as the probability of hitting more than one scattering center during the interaction with a filament is itself increased.

As the density of scattering centers in a filament becomes $n_{i|f} = n_i/f_f$, where $f_f \sim 5\%$ is the average filament filling factor in the Universe, the mean free path to interaction inside a filament becomes $f_f d_i$. Consequently, the average number of interactions $N_{\text{int}|f}$ with scattering centers of type i during the ballistic crossing of a filament of radius r_f is:

$$N_{\text{int}|f} = \frac{\pi r_f}{f_f d_i}. \quad (12)$$

In this equation, a geometrical factor $\pi/2$ accounts for the random pitch angle of the incoming particle. This formula assumes that the particle suffers a deflection angle much smaller than unity at each interaction. In the opposite diffusive regime, in which $\delta\theta_i^2 \sim 1$, the particle follows a random walk and exits the filament after $N_{\text{int}|f} \simeq [r_f/(f_f d_i)]^2$ interactions. In total, the particle exits the filament with a total deflection and time delay (with respect to straight line crossing of the filament):

$$\delta\theta_{i|f}^2 = \min(1, N_{\text{int}|f} \delta\theta_i^2), \quad (13)$$

$$\delta t_{i|f} = N_{\text{int}|f} \left(\delta t_i + \delta\theta_i \frac{f_f d_i}{c} \right). \quad (14)$$

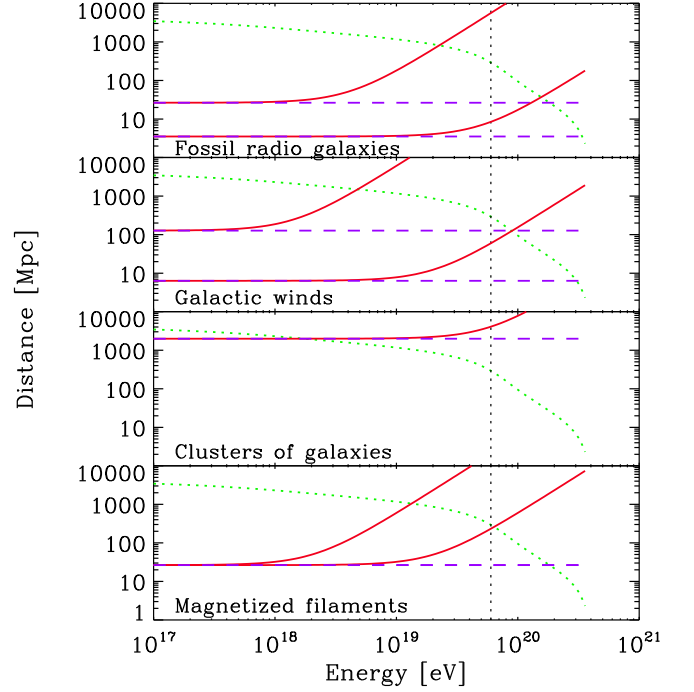


FIG. 4: Distance to the last scattering surface for different types of scattering agents and for two different sets of parameters in each case. Solid lines: scattering length l_{scatt} for deflection of order unity, as defined in Eq. (7); dashed lines: distance \bar{d} to the last scattering surface as defined in Eq. (5). The dotted (green) line indicates the source distance scale l_{max} . The vertical dotted line indicates the location of E_{GZK} . Fossil radio galaxies: $n_{\text{rg}} = 3 \cdot 10^{-3} \text{ Mpc}^{-3}$, $B_{\text{rg}} = 10^{-8} \text{ G}$, $\lambda_{\text{rg}} = 100 \text{ kpc}$, and $r_{\text{rg}} = 2 \text{ Mpc}$ (lower curves); $n_{\text{rg}} = 10^{-2} \text{ Mpc}^{-3}$, $B_{\text{rg}} = 10^{-7} \text{ G}$, $\lambda_{\text{rg}} = 100 \text{ kpc}$, and $r_{\text{rg}} = 3 \text{ Mpc}$ (upper curves). Magnetized galactic winds: $n_{\text{gw}} = 10^{-2} \text{ Mpc}^{-3}$, $B_{\text{gw}} = 10^{-8} \text{ G}$, $\lambda_{\text{gw}} = 50 \text{ kpc}$, and $r_{\text{gw}} = 0.5 \text{ Mpc}$ (lower curves); $n_{\text{gw}} = 5 \cdot 10^{-2} \text{ Mpc}^{-3}$, $B_{\text{gw}} = 10^{-7} \text{ G}$, $\lambda_{\text{gw}} = 50 \text{ kpc}$, and $r_{\text{gw}} = 0.8 \text{ Mpc}$ (upper curves). Clusters of galaxies: $n_{\text{cg}} = 10^{-5} \text{ Mpc}^{-3}$, $B_{\text{cg}} = 10^{-6} \text{ G}$, $\lambda_{\text{cg}} = 100 \text{ kpc}$, and $r_{\text{cg}} = 1 \text{ Mpc}$ (lower curves); $n_{\text{cg}} = 10^{-5} \text{ Mpc}^{-3}$, $B_{\text{cg}} = 10^{-7} \text{ G}$, $\lambda_{\text{cg}} = 100 \text{ kpc}$, and $r_{\text{cg}} = 4 \text{ Mpc}$ (upper curves). Magnetized filaments of large scale structure: interseparation $d_f = 25 \text{ Mpc}$, $B_f = 3 \cdot 10^{-9} \text{ G}$, $\lambda_f = 300 \text{ kpc}$, and $r_f = 2 \text{ Mpc}$ (lower curves); $d_f = 25 \text{ Mpc}$, $B_f = 3 \cdot 10^{-8} \text{ G}$, $\lambda_f = 300 \text{ kpc}$, and $r_f = 2 \text{ Mpc}$ (upper curves).

In these equations, $\delta\theta_i$ and δt_i denote respectively the deflection angle and time delay consecutive to an interaction with scattering center of type i , as discussed in Appendix A, while $\delta\theta_{i|f}$ and $\delta t_{i|f}$ give the corresponding deflection angle and time delay after the crossing of a filament.

Note that the filling factor of the magnetized halos in the filament is f_i/f_f , with $f_i \simeq (4/3)n_i\sigma_i r_i$ the average filling factor of scattering centers in the Universe. The filament becomes overfilled by the halos when $f_i \gtrsim f_f$, or equivalently $N_{\text{int}|f} \gtrsim (3\pi/4)r_f/r_i$. If this condition is satisfied, one needs not consider the multiple interaction scenario depicted above, as it suffices to consider the

filaments themselves as the scattering centers.

As mentioned above, the average distance to scattering is also modified if scattering centers cluster in filaments. It becomes $d_{i,f}$:

$$d_{i,f} \simeq \frac{d_f}{1 - \exp(-N_{\text{int}})}, \quad (15)$$

as the denominator in this expression represents the probability of hitting a scattering center when the particle hits a filament. The quantities $d_{i,f}$, $\delta\theta_{i|f}$ and $\delta t_{i|f}$ suffice in principle to characterize the transport of the particle in this structured Universe and to derive the phenomenological consequences with respect to experimental data. To gauge the influence of the geometry, one should compare the above quantities to those expected for a homogeneous scattering center distribution for typical values of the parameters. One finds:

$$N_{\text{int}|f} \simeq 3.9 \left(\frac{r_f}{2 \text{ Mpc}} \right) \left(\frac{f_f}{0.05} \right)^{-1} \times \left(\frac{n_i}{10^{-2} \text{ Mpc}^{-3}} \right) \left(\frac{r_i}{1 \text{ Mpc}} \right)^2. \quad (16)$$

For the fiducial values used in Eq. (16), $f_i/f_f = 0.83$, i.e. the halos barely overfill the filaments. This means that if r_i or n_i is larger than the quoted values, one must consider that the scattering centers are the filaments themselves, with the average quantities d_f , r_f and B_f discussed previously. Conversely, if r_i or n_i is smaller, one must follow the above multiple interaction scheme.

The above discussion sketches the influence of inhomogeneity on the number of interactions at each interaction with a zone of enhanced density. Since the Universe becomes roughly homogeneous and isotropic on length scales larger than ~ 100 Mpc, one should expect the number of interactions to be similar for both homogeneous and inhomogeneous scattering centers distributions on such length scales, and the discussion of Section II B 1 should remain unchanged in this limit. However, one cannot exclude a priori that the structuration of matter in the Universe could produce a sophisticated law of probability for the interaction path length, leading to non-standard effects such as anomalous diffusion.

Monte Carlo simulations of particle propagation in a “realistic” scattering center distribution are best suited to address such issues and to provide quantitative estimates of the effect of inhomogeneity on the transport.

D. Inhomogeneity of the large scale structure - Numerical simulations

We have performed such simulations using a variant of the numerical code described in Ref. [52]. The simulation of the dark matter density field has been produced by the `RAMSES` code [53], and was kindly provided to us by S. Colombi; its characteristics are 256^3 cells, with extent

280 Mpc, giving a grid size 1.1 Mpc. For each simulation, we sample a population of scattering centers. We adopt two physically motivated bias models: in the first model, the scattering center density is proportional to the dark matter density field; in the second, the same proportionality applies, but we do not allow scattering centers to reside in regions with dark matter density $\rho < 0.5\langle\rho\rangle$. This latter model enhances the segregation of scattering centers in the large scale structure.

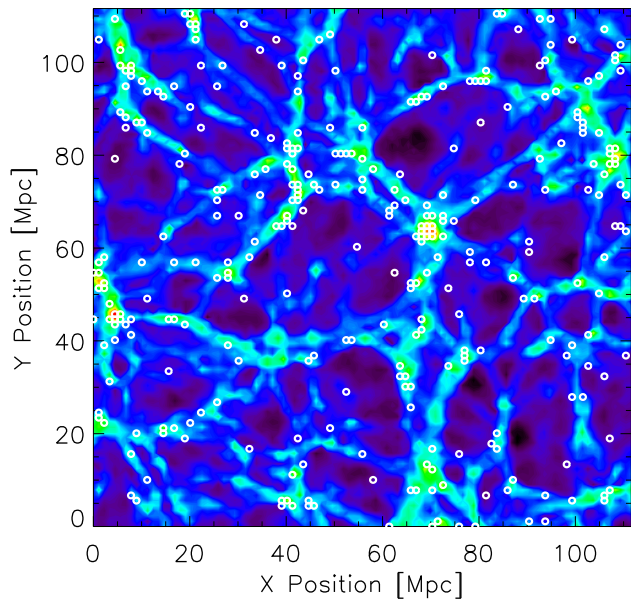


FIG. 5: Distribution of scattering centers in the large scale structure (in white), in a model in which the density of scattering centers follows that of dark matter (density contrast represented in colors). The average density is 10^{-2} Mpc^{-3} .

Figure 5 shows an example of a scattering center distribution in a two-dimensional slice of the simulation box in the first bias model. The segregation of scattering centers in filaments of the large scale structure is apparent, although some tend to reside in smaller density regions as a result of the large volume fraction occupied by such regions. Out of simplicity, each scattering center is modelled as a cube of the size of a cell of the simulation; each cell in the simulation is thus occupied by zero or one scattering center.

We then follow the trajectories of cosmic rays of various energies, using the method of Ref. [52], which simulates the transport of particles across cells of coherence of the magnetic field in both the diffusive and non-diffusive regime. These simulations allow to compute the various statistical properties of transport. A first effect brought to light by these simulations is the general increase in the length of first interaction in the inhomogeneous case, when compared to the homogeneous scattering center distribution. This increase is of order 40% for the first bias model, and about 60% for the second bias model.

It does not seem to depend strongly on the scattering center density.

Another significant effect is related to the source environment. If this latter is dense, as one might expect, the local scattering center density is higher than average, and therefore the cosmic ray may experience several interactions in the source environment in the first megaparsecs. Accordingly, the probability distribution for the first interaction departs from a simple exponential law: it exhibits a peak in the first Mpc, then decreases as an exponential. Although these extra interactions will not affect strongly the total deflection angle as seen from the detector, since 1 Mpc seen from 100 Mpc is subtended by an angle 0.6° , they will increase the time delay (with respect to straight line propagation).

This effect is apparent in Fig. 6 which shows the average number of interactions as a function of distance, for different energies. The dashed lines indicate the corresponding trends for a homogeneous scattering distribution, which go to zero when the traveled distance tends to zero. On the contrary, the solid lines, which correspond to the simulated inhomogeneous case, depart from this scaling and indicate a fixed number of interactions, of order 2. The exact number turns out to depend on the environment density and has a variance of order unity. For a source in an environment of average density, the number of such extra interactions in the source surroundings is negligible.

Figure 6 also reveals other interesting features. In particular, one can see clearly that the average number of interactions in the inhomogeneous case converges towards that obtained in the homogeneous case on distance scales $\gtrsim 100 - 200$ Mpc, as expected. For the highest energies, namely $E = 10^{19.7}$ eV and $E = 10^{20}$ eV, there is a slight offset between the analytical prediction $1/n\sigma$ and the homogeneous calculation; this difference is attributed to the cubic geometry of the scattering center. Particles of lower energies, in particular $E = 10^{19}$ eV, diffuse in the scattering center distribution, as evidenced by the higher slope of the average number of interactions as a function of the distance traveled d . One can check in particular that $N_{\text{int}} \sim (n\sigma d)^2$ as expected. At very large distances, this relation breaks down because the trajectory is cut after a time t_{max} ; hence less and less particles are able to travel beyond a distance $\sim (ct_{\text{max}})^{1/2}(n\sigma)^{-1/2}$. Similar features are observed in the second bias model.

Finally, the same simulations can be used to compute the average deflection angle as a function of energy and traveled distance. This calculation is performed as follows. At a predetermined distance d , one draws at random a certain number of “small spheres” positioned on the sphere of radius d around the source. These “small spheres” mimic the detectors located at distance d from the source. There must be a sufficient number of these “small spheres” to guarantee a sufficient signal, but not so many that they would overlap, in which case one would oversample the sphere of radius d . Each time a trajectory intersects one of these spheres, the angle between

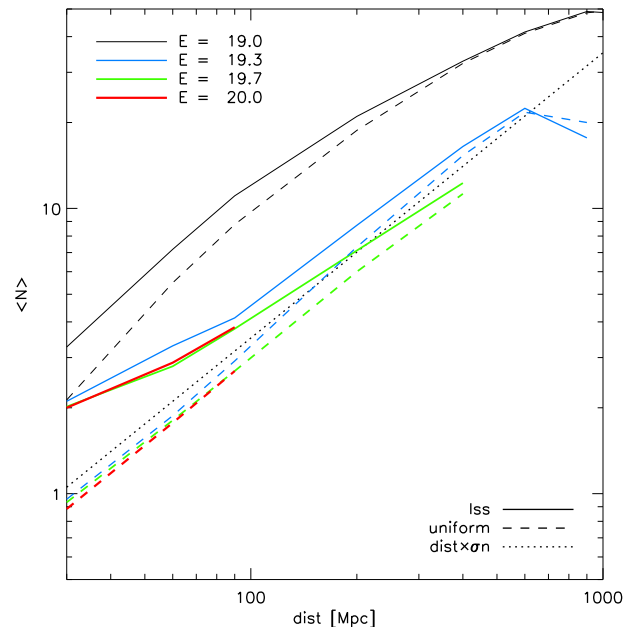


FIG. 6: Average number of interactions as a function of distance traveled in a time $t_{\text{max}}(E)$. The scattering center density is such that $(n\sigma)^{-1} = 32$ Mpc (which mimics the case $n = 10^{-2} \text{ Mpc}^{-3}$, $r = 1$ Mpc). Each scattering center is endowed with a magnetic field $B = 3 \cdot 10^{-8}$ G and coherence length $\lambda = 100$ kpc. From top to bottom, solid lines correspond to different energies (in increasing order), as indicated in the colored version.

the particle incoming direction in this sphere and the source location is recorded. Iterating over the particles and the “small spheres” allows to reconstruct the probability distribution of deflection angles. The result is shown in Fig. 7 for various energies, for the same inhomogeneous distribution of scattering centers as above. The values shown in Fig. 7 have been computed at the following distances: 1000 Mpc for $E = 10^{19}$ eV, 600 Mpc for $E = 10^{19.3}$ eV, 400 Mpc for $E = 10^{19.7}$ eV and 90 Mpc for $E = 10^{20}$ eV. These distances are representative of l_{max} hence of the source distance scale. At an energy $E = 10^{20}$ eV, the typical deflection is of order 3° , while at $E = 10^{19.7}$ eV, it increases to 12° , and becomes large at smaller energies. Obviously, these deflections could be larger or smaller depending on the exact values of the scattering center characteristics, see discussion above.

To summarize this discussion on the effect of inhomogeneity, we note the following features: when the scattering centers correlate with the large scale structure, the probability law of first interaction and the number of interactions departs from those obtained in the homogeneous case, at distances $\lesssim 100$ Mpc. The difference between the two cases depends on several factors: the source environment and the bias of the scattering center distribution with respect to the underlying dark matter distribution, in particular. It is found however that on

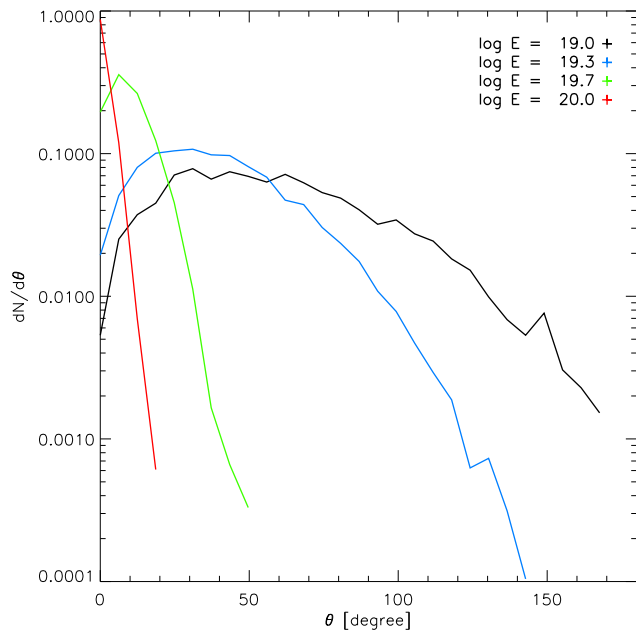


FIG. 7: Average deflection for different energies, as indicated. The values have been computed at different distances for the different energies: 1000 Mpc for $E = 10^{19}$ eV, 600 Mpc for $E = 10^{19.3}$ eV, 400 Mpc for $E = 10^{19.7}$ eV and 90 Mpc for $E = 10^{20}$ eV. As before, the scattering center density is such that $(n\sigma)^{-1} = 32$ Mpc (which mimics the case $n = 10^{-2}$ Mpc $^{-3}$, $r = 1$ Mpc). Each scattering center is endowed with a magnetic field $B = 3 \cdot 10^{-8}$ G and coherence length $\lambda = 100$ kpc.

large scales $\gtrsim 100$ Mpc, the inhomogeneity of the scattering center distribution does not play any role. Extra interactions in the source environment, if sufficiently dense to be populated by scattering centers, may increase the time delay with respect to straight line propagation but will not modify substantially the total deflection angle.

III. CONSEQUENCES FOR COSMIC RAY TRANSPORT

In this section, we discuss the phenomenological consequences of the above model of cosmic ray transport with respect to the signatures of different source models, discussing in particular the absence or existence of counterparts. We will discuss in Section IV the interpretation of existing data in the light of these consequences, and in particular the recent correlation announced by the Pierre Auger Observatory.

A. Optically thin regime

The optically thin regime, in which $l_{\max} < \bar{d} < l_{\text{scatt}}$, is trivial in terms of particle propagation: most parti-

cles travel in straight line, without interacting in the intergalactic medium, hence one should expect to see the source directly in the arrival direction of the highest energy events. As discussed briefly in the introduction, this does not seem to be the case. Extra deflection could arise from an all-pervading intergalactic magnetic field or the Galactic magnetic field.

The influence of an all-pervading intergalactic magnetic field has been discussed in previous works, see for instance Refs. [21, 22, 23, 24] for recent works. Note that our model of magnetized filaments and non-magnetized voids may be considered as an approximation to the more realistic magnetic field configurations derived in these studies.

Concerning the influence of the Galactic magnetic field, existing models suggest that the typical deflection at the highest energies, say $\simeq 10^{20}$ eV, are probably of the order of a few degrees [54, 55]. Hence one would need to invoke the existence of an extended magnetized halo to provide sufficient deflection. Alternatively, one may consider a scenario in which most particles at the highest energies are heavy nuclei, which are more easily deflected.

B. Intermediate regime

The intermediate regime, in which $\bar{d} < l_{\max} < l_{\text{scatt}}$ is interesting, because the typical deflection is smaller than unity, yet it could be sufficient to explain the lack of counterpart.

1. Transport

Since the total deflection remains smaller than unity, one may describe the transport as near-ballistic with a non-zero time delay as measured relatively to straight line propagation. Furthermore, one may use in this case the time delay and deflection formulae obtained from random walk arguments in Ref. [49, 56], provided one accounts for the inhomogeneity of the magnetic field. In detail, at each scattering with scattering center i , the particle suffers and angular deflection $\delta\theta_i$ and exits with a delay δt_i . The formula for $\delta\theta_i$ is given in Eq. (A3), while the expression for δt_i can be obtained as:

$$\delta t_i \simeq 150 \text{ yr} \left(\frac{r_i}{1 \text{ Mpc}} \right)^2 \left(\frac{B}{10^{-8} \text{ G}} \right)^2 \times \left(\frac{\lambda_i}{0.1 \text{ Mpc}} \right) \left(\frac{E}{10^{20} \text{ eV}} \right)^{-2}. \quad (17)$$

Recall that λ_i represents the coherence length of the magnetic field in structure i and r_i the extent of this latter. The total time delay τ acquired over a path length l is given by the sum of the time delays acquired during each scattering as well as that resulting from the fact that the particle does not travel in a straight line from the source

to the detector. On average, the particle interacts at every step of length \bar{d} , with probability \bar{d}/d_i of hitting a structure of type i . Then the time delay and deflection acquired after traveling a path length l are:

$$\delta\theta^2 = \frac{l}{\bar{d}} \sum_i \frac{\bar{d}}{d_i} \delta\theta_i^2, \quad (18)$$

$$\tau \simeq \frac{l}{\bar{d}} \sum_i \frac{\bar{d}}{d_i} \delta t_i + \frac{l\delta\theta^2}{4c}. \quad (19)$$

To make simple estimates, consider the case in which one type of scattering event dominates the scattering history. Then the typical deflection angle reads:

$$\begin{aligned} \delta\theta \simeq & 3.0^\circ \left(\frac{l}{100 \text{ Mpc}} \right)^{1/2} \left(\frac{n_i}{10^{-2} \text{ Mpc}^{-3}} \right)^{1/2} \times \\ & \left(\frac{r_i}{1 \text{ Mpc}} \right)^{3/2} \left(\frac{B_i}{10^{-8} \text{ G}} \right) \times \\ & \left(\frac{\lambda_i}{0.1 \text{ Mpc}} \right)^{1/2} \left(\frac{E}{10^{20} \text{ eV}} \right)^{-1}. \end{aligned} \quad (20)$$

This deflection may thus be non-negligible for typical parameters of the scattering centers discussed in the previous section. In all cases, the arrival direction should point back to the last scattering center encountered by the cosmic ray. Since scattering centers are highly magnetized regions, and as such are probably associated with active objects such as radio-galaxies, one may be deceived by their presence on the line of sight, and interpret them as the source of ultra-high energy cosmic rays. The smoking gun of such counterfeiting is the distance scale to these objects: in this optically thick regime, most counterparts would be located at a distance scale \bar{d} (which can be measured) significantly smaller than the expected distance scale l_{max} (which is known).

The associated time delay reads:

$$\tau \simeq 0.2 \cdot 10^6 \text{ yrs} \left(\frac{l}{100 \text{ Mpc}} \right) \left(\frac{\delta\theta}{3^\circ} \right)^2. \quad (21)$$

The second term on the r.h.s of Eq. (19) indeed dominates largely over the first. Note furthermore that this time delay may be slightly increased if extra interactions occur in the source environment as discussed in Section II D.

2. Experimental signatures for continuously emitting sources

As far as continuously emitting sources are concerned, a possibly large angular deflection could prevent the detection of counterparts. Indeed, values such as $n_i = 10^{-2} \text{ Mpc}^{-3}$, $r_i = 1 \text{ Mpc}$ and $B_i = 10^{-8} \text{ G}$ suffice to produce a deflection of order 17° over a path length $l = l_{\text{max}}$ at energy $4 \cdot 10^{19} \text{ eV}$, which is a generic threshold energy used in the search for counterparts. The strong evolution of $\delta\theta$ with energy results from the strong evolution

of l_{max} with E close to the threshold for pion production. This suggests that counterparts should be found at sufficiently high energies, which of course asks for high statistics.

Since the flux received from sources within distance l scales as l , one may expect to see the source in the arrival directions of a subset l_0/l_{max} of all events, l_0 being defined as the distance at which the typical deflection becomes comparable to the radius within which one searches for counterparts. This number l_0/l_{max} should be smaller than unity, since if it were unity, it would mean that the total angular deflection for all sources is very small, hence that counterparts should have been detected.

3. Experimental signatures for bursting sources

Regarding bursting sources, and gamma-ray bursts in particular, Eq. (21) shows that the typical time delay is sufficiently large to explain the lack of temporal association between cosmic ray arrival directions and gamma-ray bursts, as well as the continuous rate of detection of high energy cosmic rays. Recall indeed that one potential difficulty of the gamma-ray burst scenario is to explain the near continuous detection of cosmic rays at the highest energies $\sim 10^{20} \text{ eV}$, when the gamma-ray burst rate is only $\sim 10^{-3} \text{ yr}^{-1}$ within the energy loss distance $\sim 100 \text{ Mpc}$. As noted by Waxman [56], this difficulty may be overcome if the arrival time spread $\Delta\tau$ of the highest energy events is sufficiently large, i.e. $\Delta\tau \gtrsim 10^3 \text{ yr}$ at 10^{20} eV in particular. Previous studies have computed this time spread under the assumption that angular deflection is a continuous process. In the present case, deflection occurs as a sequence of random events, which modifies the discussion.

Following Ref. [49], we note that the magnitude of $\Delta\tau/\tau$ is influenced by the number of different trajectories that the particle can follow from the source to the detector. If indeed all particles follow the very same trajectory, $\Delta\tau \rightarrow 0$, while if different particles may follow different trajectories, one should expect $\Delta\tau \sim \tau$. In the present model, the former situation prevails if the typical displacement $l\delta\theta$ away from the line of sight is smaller than the mean free path to scattering, i.e. $l\delta\theta \ll \bar{d}$; the latter situation prevails in the opposite limit. The fiducial parameters used in Eq. (21) indicate $l\delta\theta < \bar{d}$, hence $\Delta\tau \ll \tau$. In this case, the broadening of the time signal at the highest energies is likely to be dominated by the influence of stochastic pion production, which results in $\Delta\tau/\tau \sim 1$ [57]. A more accurate measurement of $\Delta\tau/\tau$ could be carried out through numerical Monte Carlo simulations, see Ref. [57].

One may also calculate the number of gamma-ray bursts sources which can contribute to the flux at a given energy E [49, 58]:

$$N_{\text{GRB}}(E) \simeq \dot{n}_{\text{GRB}} \frac{2\pi}{5} l_{\text{max}}^3 \Delta\tau. \quad (22)$$

This number of apparent gamma-ray bursts in the cosmic ray sky characterizes the amount of statistical fluctuation to expect around the mean flux at a given energy [49]. Using Eq. (21), one obtains:

$$N_{\text{GRB}}(E) \simeq 0.3 \times 10^3 \left(\frac{l_{\text{max}}}{100 \text{ Mpc}} \right)^5 \left(\frac{E}{10^{20} \text{ eV}} \right)^{-2} \times \left(\frac{n_i}{10^{-2} \text{ Mpc}^{-3}} \right) \left(\frac{r_i}{1 \text{ Mpc}} \right)^3 \times \left(\frac{B_i}{10^{-8} \text{ G}} \right)^2 \left(\frac{\lambda_i}{0.1 \text{ Mpc}} \right) \times \left(\frac{\dot{n}_{\text{GRB}}}{10^{-9} \text{ Mpc}^{-3} \cdot \text{yr}^{-1}} \right) \frac{\Delta\tau}{\tau}. \quad (23)$$

This number is large, even at the highest energies where $\Delta\tau/\tau \sim 1$ due to pion production. This implies that the spectrum of ultra-high energy cosmic rays should not reveal statistical fluctuations until energies as large as a few 10^{20} eV.

At energies below the pion production threshold, where l_{max} increases rapidly to large values, one expects $l\delta\theta$ to become larger than \bar{d} , hence $\Delta\tau \sim \tau$. Since this ratio $\Delta\tau/\tau$ characterizes the width of the angular image, the rapid variation of $\Delta\tau/\tau$ with energy should produce interesting angular images of a given burst (provided a multiplet with sufficient multiplicity can be observed). In more detail, as $\Delta\tau/\tau \ll 1$, $\delta\theta$ characterizes a systematic offset of the apparent image from the source location, but the image should reveal a small angular size $\Delta\theta \ll \delta\theta$. In the limit $\Delta\tau/\tau \sim 1$, $\delta\theta$ rather characterizes the typical width the angular image, which should be centered on the source location. In the intermediate regime, one may expect several source images [49] [see also Ref. [59] for a demonstration of magnetic lensing of high energy cosmic rays].

C. Optically thick regime

The optically thick or opaque regime corresponds to $\tau > \tau_{\text{eff}} > 1$. In this case, cosmic rays diffuse from the source to the detector as in a random billiard.

1. Transport

Assuming that the diffusion process obeys the normal law $\langle r^2 \rangle = 2Dt$, one may calculate the diffusion coefficient D using random walk arguments. In particular, if one neglects the time spent in a magnetized structure in the course of an interaction, the diffusion coefficient is related to the scattering length via the usual law: $D = l_{\text{scatt}}c$, where the scattering length l_{scatt} has been defined in Eq. (7) above.

If the particle diffuses inside a structure during an interaction, then it actually gets trapped in this structure during a certain amount of time and exits backwards in a

mirror-like fashion (see Appendix A). Consider for simplicity a single scattering agent. One may then account for the effect of time trapping by counting the effective time taken to accomplish N steps of the random walk, which becomes $Nd_i(1 + \delta t_i c/d_i)/c$. The correction decreases D by a factor $(1 + \delta t_i c/d_i)$. Since the trapping time $\delta t_i \simeq r_i/c$ is smaller than the typical distance d_i between two scattering centers, this correction is not dominant. Concerning the effect of mirroring, it suffices to note that it takes two interactions to achieve isotropic deflection, hence this decreases the diffusion coefficient by another factor of 2. These two corrections thus remain of order unity.

The general scaling of this diffusion coefficient with energy is easily grasped. At low energies (typically $E \lesssim 10^{18}$ eV depending on the parameters characterizing the scattering agents), it does not depend on energy, as l_{scatt} simply corresponds to the mean free path for scattering \bar{d} . In the high energy regime, $D \propto E^2$ since the number of scatterings to achieve a deflection of order unity scales in the same way. The above diffusion coefficient may be used to describe the propagation of particles, as done in Refs. [52, 60, 61, 62, 63].

In principle, a realistic distribution of magnetic field cells inside the large scale structure might induce a scattering law with a more complex profile than the standard exponential form adopted here, which would furthermore depend on time in a non-trivial way so as to account for the effect of trapping. The particle would then follow a so-called continuous time random walk with waiting times, the properties of which can be derived by following the methods developed in Refs. [64, 65]. It would certainly be particularly interesting if anomalous diffusion laws were to occur in such magnetic field configurations.

2. Experimental signatures for continuously emitting sources

The arrival direction of high energy events will point back to the source only if this latter is located at a distance closer than l_{scatt} . In the diffusive regime, the source distance scale is no longer l_{max} but $\sqrt{l_{\text{scatt}}l_{\text{max}}}$, since this latter gives the distance that a particle can cross before losing its energy. Since we assume $l_{\text{max}} > l_{\text{scatt}}$, most of the sources are located beyond l_{scatt} .

In the steady state regime, the diffusive flux received from a source at distance l scales as $1/(l_{\text{scatt}}l)$, hence the flux received from sources within l , with $l > l_{\text{scatt}}$, scales as l^2/l_{scatt} . Consequently, the fraction of the flux that can be received from sources at distances closer than l_{scatt} [given by Eq. (10)] is roughly $l_{\text{scatt}}/l_{\text{max}}$, just as in the non-diffusive regime. This fraction gives the fraction of events behind which one can hope to detect the source.

Note that the same delusive effect of finding a scattering center in the arrival direction of cosmic rays occurs in this regime just as in the semi-transparent regime.

One can calculate the expected number of events mul-

triplets as follows. Since most cosmic rays originate from a distance larger than l_{scatt} , the expected *average* multiplicity, \bar{N}_m , is given by the ratio of the total number of events detected, \bar{N}_{obs} , to the number of scattering agents on the surface of large angular scattering (i.e. at distance l_{scatt}). This gives:

$$\bar{N}_m \sim 10^{-5} N_{\text{obs}} \left(\frac{l_{\text{scatt}}}{100 \text{ Mpc}} \right)^{-3} \left(\frac{n_i}{10^{-2} \text{ Mpc}^{-3}} \right)^{-1}. \quad (24)$$

In this equation, n_i represents the average scattering center density. Unless l_{scatt} is smaller than ~ 10 Mpc, and N_{obs} sufficiently large, it appears unlikely to see a doublet or even a triplet in a given arrival direction.

However, sources within the sphere of large angular scattering (for which the Universe appears semi-transparent) may produce images with higher multiplicity if they exist, i.e. if $n_s^{-1/3} < l_{\text{scatt}}$. The number of events expected from a source at distance l can be written as:

$$N_m \simeq \frac{N_{\text{obs}} f_{\text{fov}}}{n_s 4\pi l^2 l_{\text{max}}}. \quad (25)$$

In order to derive this estimate, it suffices to express the flux received from this source, and to replace \dot{N}_{UHECR} in this expression using Eq. (10). The parameter f_{fov} gives the fraction of time during which the source remains in the field of view of the experiment, as measured relatively to the total integration time. Since $N_m \propto 1/l^2$, the maximum multiplicity N_1 will be associated to the closest source at distance $\sim n_s^{-1/3}$:

$$N_1 \simeq 0.1 f_{\text{fov}} N_{\text{obs}} \frac{n_s^{-1/3}}{l_{\text{max}}}. \quad (26)$$

To provide quantitative estimates, if $n_s = n_{s,-6} \times 10^{-6} \text{ Mpc}^{-3}$, the number of events expected from the closest source at energies greater than $4 \times 10^{19} \text{ eV}$ is a fraction $0.02 f_{\text{fov}} n_{s,-6}^{-1/3}$ of all observed events. This number of events becomes a fraction $0.03 f_{\text{fov}} n_{s,-6}^{-1/3}$ of N_{obs} above $6 \times 10^{19} \text{ eV}$. The AGASA experiment has reported the observation of 72 events above $4 \times 10^{19} \text{ eV}$ [73]; in this case, one would expect $N_1 \simeq f_{\text{fov}} n_{s,-6}^{-1/3}$ if $n_s^{-1/3} < l_{\text{scatt}}$. This number agrees with the reported typical multiplicity $\sim 2 - 3$ if $f_{\text{fov}} \sim 1$ and $n_{s,-6} \sim 1$. Note that the expected multiplicity is the same in this case than that found in the absence of magnetic fields, since we assume the source to be within the sphere of large angular scattering.

3. Experimental signatures for bursting sources

As far as bursting sources such as gamma-ray bursts are concerned, most of the above results remains unchanged; one simply has to replace $n_s \dot{N}_{\text{UHECR}}$ with $\dot{n}_s \dot{N}_{\text{UHECR}}$. In the present case, the typical time spread

corresponds to the diffusive travel time, i.e. for a source at distance l :

$$\Delta t \simeq \frac{l^2}{2l_{\text{scatt}} c}. \quad (27)$$

Therefore the number of gamma-ray bursts sources which can contribute to the flux at a given energy E , at any time, is:

$$N_{\text{GRB}} \simeq \dot{n}_s \frac{2\pi}{5} \frac{l_{\text{max}}^5}{l_{\text{scatt}} c}. \quad (28)$$

To make concrete estimates, at 10^{20} eV , $l_{\text{max}} \simeq 95 \text{ Mpc}$ hence $N_{\text{GRB}} \sim 20$ if $l_{\text{scatt}} = 20 \text{ Mpc}$, assuming $\dot{n}_s = 10^{-9} \text{ Mpc}^{-3} \text{ yr}^{-1}$. N_{GRB} is larger than unity, which implies that one should not detect significant statistical fluctuation in the energy spectrum and which explains why one can record cosmic ray events in a near continuous manner, despite the fact that close-by gamma-ray bursts are such rare events.

There will of course be an energy E_c where $l_{\text{scatt}} = l_{\text{max}}$, beyond which the diffusive regime will no longer apply. In this case, one must use the formulae given in Section III B for the semi-transparent regime. Similarly, regarding sources located within the sphere of large angular scattering, i.e. at a distance $l < l_{\text{scatt}}$, the phenomenological consequences are those described in Section III A if $l < \bar{d}$, or in Section III B if $\bar{d} < l < l_{\text{scatt}}$.

IV. DISCUSSION

A. Summary of present results

The present work has provided a new description of ultra-high cosmic ray transport in highly inhomogeneous magnetic fields. The corresponding configuration of the extragalactic magnetic field is that of a collection of scattering centers, such as halos of radio-galaxies or starburst galaxies, or magnetized filaments, with a negligible magnetic field in between. Such a configuration is generally expected in scenarios in which the magnetic field is produced and ejected by a sub-class of galaxies, or generated at the accretion shock waves of large scale structure. Even if the magnetic field is rather generated at high redshift, subsequent amplification in the shear and compressive flows of large scale structure formation tends to produce a highly structured configuration, with strong fields in the filaments of galaxies and weak fields in the voids [21, 22, 23, 24].

In our description, transport of cosmic rays is modeled as a sequence of interactions with the scattering centers, during which the particle acquires a non-zero deflection angle and time delay (with respect to straight line crossing of the magnetized region), see Appendix A. In Section II, we have sketched a list of possible scattering centers and their characteristics (mean free path to scattering, magnetic field, coherence length and extent). We have then computed the optical depth τ of

the Universe to cosmic ray scattering as a function of energy and distance to the source, as well as the effective optical depth τ_{eff} (which is defined in such a way as to become unity when the total angular deflection becomes unity). As discussed in Section II, the Universe can be semi-transparent to cosmic rays if $\tau > 1 > \tau_{\text{eff}}$, meaning that the total deflection is smaller than unity but non-zero, opaque, i.e. if $\tau > \tau_{\text{eff}} > 1$, or even transparent $1 > \tau > \tau_{\text{eff}}$. For typical values of the scattering centers parameters, it is expected that the Universe be semi-transparent or opaque on the source distance scale and at energies close to the pion production threshold. Since this energy is that generally used by experiments as a threshold for the search for counterparts, the above may have important phenomenological consequences.

In particular, in the semi-transparent or opaque regime, the closest object lying in the cosmic ray arrival direction should be a scattering center. Since these scattering centers are sites of intense magnetic activity (radio-galaxies, starburst galaxies, shock waves, ...), they might be mistaken with the source. This peculiar feature does not arise in models in which magnetic deflection is a continuous process in an all-pervading magnetic field. One could thus conceive an “ironic” scenario, in which cosmic rays are accelerated in gamma-ray bursts, but scatter against radio-galaxies magnetized lobes, so that one interpret these latter as the source of cosmic rays because they are the only active objects seen on the line of sight. If such counterfeiting is taking place, one should observe that the apparent distance scale to the source (actually the distance to the last scattering surface) is smaller than the expected distance scale to the source (determined by the energy losses). This offers a simple way to test for the above effect.

In the semi-transparent regime, the source is displaced from the arrival direction by a non-zero (yet smaller than unity) deflection angle. Increasing the threshold energy above which one searches for counterparts certainly provides the way to evade this magnetic effect and identify the source. Indeed, as shown in Section II, the optical depth falls rapidly with increasing energy, in combination of the decreasing distance scale to the sources (which is limited by energy losses) and the decreasing deflection angle per scattering. Furthermore, a fraction $\exp(-\tau)$ of all events should have suffered negligible deflection in the intergalactic magnetic field. Hence it appears important to consider searches for counterparts on an event by event basis, focusing on events with extreme energies $> 10^{20}$ eV, rather than a statistical correlation with astrophysical catalogs. This, however, requires large aperture experiments such as Auger North [74] in view of the strongly decreasing flux at the highest energies.

Although most of the discussion has assumed that the scattering centers are homogeneously distributed in the intergalactic medium, we have discussed the case of inhomogeneous distributions in Sections II C, II D, on the basis of both analytical and numerical arguments. In particular, it is found numerically that on path lengths

longer than ~ 100 Mpc, the effect of inhomogeneity is negligible, as expected for a Universe that is homogeneous and isotropic on these scales. The path length to the first interaction is generally higher by about 40% than in the homogeneous case if the scattering centers distribute according to the dark matter density. Since scattering centers tend to concentrate in filaments of large scale structure, a particle may also experience multiple interactions upon crossing a filament. This explains why the number of interactions in the inhomogeneous case converges towards that of the homogeneous case on long path lengths.

B. Recent data from the Pierre Auger Observatory

In its first years of operation, the Pierre Auger Observatory has already achieved the largest aperture (in $\text{km}^2 \cdot \text{str} \cdot \text{yr}$) [1], and it has recently released the largest catalog of events above $5.7 \cdot 10^{19}$ eV [2]. In this catalog, 20 out of 27 events originate from within 3 degrees of an active galactic nucleus located within 75 Mpc. One may offer several levels of interpretation for this correlation.

The most straightforward interpretation is to infer that active galactic nuclei are the sources of ultra-high energy cosmic rays. However, only one of the observed counterparts is of the FR-I type (Centaurus A), all others are more common Seyfert galaxies. From a theoretical point of view, this is unexpected, since these common active galactic nuclei do not seem to offer the required characteristics for the acceleration to ultra-high energies [66]. Even Centaurus A, as far as its jets are concerned, does not appear to be a likely source of ultra-high energy cosmic rays [67].

Furthermore, on a purely experimental level, Gorbunov and co-authors [68] have recently pointed out an anomaly in this observed correlation. Assuming that the AGN seen in the arrival directions of these high energy events are the source of ultra-high energy cosmic rays, these authors have computed the expected flux using the known distances to these AGN. They have observed that the Pierre Auger Observatory has collected zero event in the direction to the Virgo cluster, whereas at least six should be expected on the basis of the large concentration of AGN in this direction and the small distance scale (assuming that the cosmic rays coming from Centaurus A indeed originate from this object). As argued in Ref. [68], this observation thus rules out the possibility that AGN are the sources of ultra-high energy cosmic rays, unless the cosmic rays seen in the direction to Centaurus A come from further away. However, one may also ponder on the possibility that the Galactic magnetic field would exhibit a particular configuration in the direction to Virgo (which lies towards the Galactic North Pole), which would prevent cosmic rays from penetrating from this direction. Hence at present, one cannot exclude formally that AGN are the source of ultra-high energy cosmic rays, but the data of the Pierre Auger Observatory cannot be argued

to sustain this hypothesis strongly either.

Another interpretation suggests that the source of ultra-high energy cosmic rays clusters with the large scale structure, as AGN do, hence the observed correlation with AGN is a coincidence. This hypothesis deserves to be more carefully studied, for instance by performing cross-correlations of the observed arrival directions with galaxy catalogs, or by following the method introduced in Ref. [69]. However, assuming that the sources are located close to the AGN which have been seen in the arrival directions should not resolve the flux anomaly noted in Ref. [68], also it might mitigate it somewhat.

A third interpretation is to assume that at least part of the observed correlation is accidental because the scattering centers on the last scattering surface cluster with the large scale structure, hence with AGN. This would alleviate this flux anomaly, since the sources would no longer have to be associated with the AGN distribution. In particular, the events seen to arise from the Centaurus A complex might have been deflected in its vicinity.

As mentioned previously, this scenario can be tested by comparing the expected source distance scale with the counterpart distance scale. Interestingly, both do not match, as the source distance scale for particles with observed energy 6×10^{19} eV is of the order of 200 Mpc, significantly larger than the maximum distance of 75 Mpc for the observed counterparts. This fact has been noted in Ref. [2]; it remained mostly unexplained, although it was suggested in this work that both distance scales would agree if the energy scale were raised by 30%.

More quantitatively, one can calculate the probability that a given event with a given observed energy originates from a certain distance, using the fraction of the flux contributed by sources within a certain distance at a certain energy. This probability law can be calculated using the techniques developed in Ref. [70], then tabulated. It is then possible to calculate the probability of seeing 20 out of 27 events from a source located within 75 Mpc using the events energies reported in Ref. [2]. This probability is small, about 3%; the mean lies at 15 events out of 27 coming from within 75 Mpc. If one restricts the set of events to those that lie outside the Galactic plane ($|b| > 12^\circ$), with 19 out of 21 seen to correlate, the probability becomes marginal, of order 0.1% (the mean lies at 12 out of 21 within 75 Mpc). Finally, if one restricts oneself to the second set of events collected after May 27 2006, and on those which lie outside of the Galactic plane, with 9 out of 11 seen to correlate, the probability becomes of order 10%, with a mean at 7 out of 11 within 75 Mpc. In this latter case, the signal is less significant, but the statistics is also smaller. Since the above estimates do not take into account the uncertainty on the energy, and since they assume continuous instead of stochastic energy losses, these numbers should be taken with caution.

Nevertheless, this discussion suggests that, unless the energy scale is too low or an experimental artefact is present, the inferred distance scale to the source appears smaller than the expected source distance scale. In light

of the analysis developed in the present paper, this thus suggests that part of the correlation, if not all, may actually pinpoint scattering centers correlating with AGN rather than the source of ultra-high energy cosmic rays. *Said otherwise, the Pierre Auger Observatory may be seeing, at least partly, the last scattering surface of ultra-high energy cosmic rays, rather than the source population.* This possibility will be either confirmed or infirmed by the acquisition of a larger set of events.

In this framework, it becomes imperative to probe the arrival directions on an event by event basis, focussing on the most energetic events. In the catalog reported in Ref. [2], there is only one event above 10^{20} eV, whose arrival direction has a relatively small super-Galactic latitude, $b_{SG} \simeq -6.5^\circ$. In the above scenario, one should expect to find a scattering center on the line of sight, hence it should prove useful to perform a deep search in this direction in the radio domain, looking for traces of synchrotron emission that would attest of the presence of a locally enhanced intergalactic magnetic field. More events at higher energies, as expected from future detectors, will certainly help in this regard.

Acknowledgments

We thank S. Colombi for providing the dark matter simulation and H. Atek, G. Boue, N. Busca, Y. Dubois, A. Olinto and C. Pichon for discussions.

APPENDIX A: PARTICLE – SCATTERING CENTER INTERACTION

This section describes the interaction between a particle and a scattering center in the large scale structure, then computes the deflection angle and the trapping time in the structure before its return to non-magnetized voids. We consider both the cylindrical geometry, which is representative of an interaction with a filament, and the spherical geometry, which we use to model the interaction with a magnetized wind or cocoon. The solution of the diffusion equation in a planar geometry can be found in Ref. [59].

This discussion assumes that the magnetic field strength and the diffusion coefficient are uniform in the scattering center. Expectations in the more general non-uniform case are discussed briefly at the end of this Appendix.

1. Non diffusive interaction with a sphere or a filament

If the scattering length l_{sc} of the particle in the scattering center is much larger than the characteristic size r , the particle is simply deflected by an angle $\delta\theta$ and

emerges after a crossing time $\delta t \simeq r/c$. The characteristic size r should be thought of as the smallest length scale of the structure, i.e. the radius r_s for a sphere or the radius r_f of a cylinder.

The deflection angle at each interaction can be computed as follows. Consider a spherical magnetized halo of radius r , magnetic field B and magnetic coherence length λ . The magnetic scattering length l_{sc} of a particle of Larmor radius r_L in this structure determines the length beyond which the particle has experienced a deflection of order unity. Hence, if $l_{sc} \ll r$, the particle undergoes diffusion in the structure so that $\delta\theta_i \sim \mathcal{O}(1)$. In the following Section, it is also shown that the distance traveled in the structure is very small as compared to r , so that escape takes place close to the point of entry with a mirror-like deflection of order π (to within $\pm\pi/2$).

If, however, $l_{sc} \gg r$, the particle is only weakly deflected. In order to calculate $\delta\theta^2$, one must specify l_{sc} as a function of r_L and λ . The general relationship between these quantities can be expressed as:

$$l_{sc} \simeq \alpha r_L \left(\frac{r_L}{\lambda} \right)^\beta. \quad (\text{A1})$$

This equation neglects a numerical prefactor of order unity (see Ref. [67] for more details). The coefficient α is directly related to the level of turbulence in the structure:

$$\alpha = \left(\frac{\delta B^2}{B^2} \right)^{-1}, \quad (\text{A2})$$

where δB represents the turbulent component and B the total magnetic field. In the following, we assume $\alpha \simeq 1$, meaning full turbulence, but the calculations that follow may be generalized to $\alpha \neq 1$ without difficulty. The various scenarios of magnetic pollution discussed before do not favor the existence of significant coherent components of the magnetic field.

Regarding the exponent β , $\beta = 1$ if $r_L \gg \lambda$ [67, 71, 72]. If, however, $r_L \ll \lambda$, then β also depends on the shape of the turbulence spectrum. For instance, $\beta = -2/3$ for Kolmogorov turbulence, $\beta = 0$ for scale invariant turbulence (Bohm regime). For simplicity, and in the absence of any knowledge of the turbulence spectrum in the scattering centers, we assume $\beta = 0$, which allows to simplify the discussion. Again, it is possible to

extend the discussion to different values of β , albeit at the price of slightly more complicated expressions.

Therefore, one finds the following deflection angle. If $r_L \ll \lambda$, then $l_{sc} \simeq r_L \ll \lambda < r$, hence the particle diffuses in the structure and exits with a deflection of order unity. Note that the inequality $\lambda < r$ simply states that the coherence length of the magnetic field cannot exceed the size of the magnetic structure.

If $r_L \gg \lambda$, then $l_{sc} \simeq r_L^2/\lambda$. One then must consider whether r_L is larger or smaller than $\sqrt{\lambda r}$. In the former case, $l_{sc} \gg r$, hence the particle exits with a small deflection angle $\delta\theta^2 \simeq r\lambda/r_L^2$. In the latter case, $l_{sc} \ll r$ hence the particle exits with a deflection angle of order unity.

In conclusion, the deflection angle can be written in the approximate form:

$$\delta\theta^2 \simeq \left(1 + \frac{r_L^2}{r\lambda} \right)^{-1}. \quad (\text{A3})$$

Although this form is only approximate, it interpolates smoothly between the two different regimes of interest $r_L \ll \sqrt{r\lambda}$ (large deflection) and $r_L \gg \sqrt{r\lambda}$ (small deflection).

2. Diffusive interaction with a filament

If $l_{sc} \ll r_f$, the particle diffuses inside the filament before escaping. One can assume that the particle penetrates a length scale l_{sc} inside the filament, and then enters the diffusive regime. The time-dependent diffusion equation can then be used to compute the probability of escape as a function of time, treating the point of first interaction (at depth l_{sc}) as an impulsive source. To this effect, we describe the filament as a cylinder of radius r_f and infinite extension along z and consider cylindrical coordinates (r, θ, z) . For simplicity, we assume a spatially uniform diffusion coefficient D_\perp in the plane perpendicular to z , and a spatially uniform diffusion coefficient D_\parallel in the direction along z . We also neglect energy losses, which is justified in so far as we will show that the trapping time is short on the typical energy loss timescale. The equation for the Green's function $g(r, \theta, z, t; r_0, \theta_0, z_0, t_0)$ reads:

$$\partial_t g - D_\perp \frac{1}{r} \partial_r (r \partial_r g) - D_\perp \frac{1}{r^2} \partial_\theta^2 g - D_\parallel \partial_z^2 g = \frac{1}{r} \delta(z - z_0) \delta(r - r_0) \delta(\theta - \theta_0) \delta(t - t_0). \quad (\text{A4})$$

Here, r_0, θ_0, z_0 and t_0 give the coordinates of the first interaction in the filament. One must also take into account the appropriate boundary conditions, namely that beyond radius r_f , the volume is unmagnetized. In the theory of diffusion, such boundary condition can be modeled by ensuring that the solution to the diffusion equation vanishes at a radius r_f . In order to solve the diffusion equation in cylindrical coordinates under this constraint, one expands the angular part of the Green's function g over a basis of proper functions of the operator ∂_θ^2 and the radial part over a basis of Bessel functions $J_m(\alpha_{ms} r/r_f)$, where α_{ms} denotes the s -th root of J_m . This guarantees that the boundary

condition will be satisfied. The solution of Eq. (A4) reads:

$$g(r, \theta, z, t; r_0, \theta_0, z_0, t_0) = \frac{1}{\pi r_f^2} \sum_{m=-\infty}^{m=+\infty} \sum_{s=1}^{s=+\infty} e^{im(\theta-\theta_0)} e^{-\alpha_{ms}^2 \frac{D_\perp |t-t_0|}{r_f^2}} \frac{e^{-\frac{|z-z_0|^2}{4D_\parallel |t-t_0|}}}{\sqrt{4\pi D_\parallel |t-t_0|}} \times \frac{J_m\left(\alpha_{ms} \frac{r_0}{r_f}\right) J_m\left(\alpha_{ms} \frac{r}{r_f}\right)}{J_{m+1}(\alpha_{ms})^2}. \quad (\text{A5})$$

The probability of having the particle inside the filament at any time $t > t_0$ is then given by the volume average of g over the filament:

$$P_{\text{res}}(t; t_0) = \int dv g = \sum_{s=1}^{s=+\infty} e^{-\alpha_{0s}^2 \frac{D_\perp |t-t_0|}{r_f^2}} \frac{2}{\alpha_{0s}} \frac{J_0\left(\alpha_{0s} \frac{r_0}{r_f}\right)}{J_1(\alpha_{0s})}. \quad (\text{A6})$$

Through the explicit decomposition of unity over the above basis of Bessel functions, one can verify that $P_{\text{esc}}(t \rightarrow t_0) = 1$ as it should. The form of $P_{\text{res}}(t; t_0)$ tends to suggest that escape takes place on a diffusive timescale r_f^2/D_\perp ; this statement is actually too naive, as shown in the following. The average residence time in the filament δt_f is calculated as:

$$\delta t_f = \int_{t_0}^{+\infty} dt P_{\text{res}}(t; t_0) = \frac{r_f^2}{2D_\perp} \sum_{s=1}^{s=+\infty} \frac{4}{\alpha_{0s}^3} \frac{J_0\left(\alpha_{0s} \frac{r_0}{r_f}\right)}{J_1(\alpha_{0s})}. \quad (\text{A7})$$

The factors in the sum on the r.h.s. of Eq. (A7) are much smaller than unity because the particle cannot penetrate further than $l_{\text{sc}} \ll r_f$ into the filament before starting to diffuse, hence $r_0 \simeq r_f(1 - l_{\text{sc}}/r_f)$. This substitution followed by the expansion of the Bessel functions to first order in terms of l_{sc}/r_f leads to the trapping time:

$$\delta t_f \simeq \frac{r_f l_{\text{sc}}}{D_\perp} \sum_{s=1}^{s=+\infty} \frac{2}{\alpha_{0s}^2}, \quad (\text{A8})$$

which is effectively smaller than the diffusive time by a factor l_{sc}/r_f . Since $D_\perp = \frac{1}{2} l_{\text{sc}} c$, one finally obtains:

$$\delta t_f \simeq \frac{r_f}{c} \sum_{s=1}^{s=+\infty} \frac{4}{\alpha_{0s}^2} = \frac{r_f}{c}. \quad (\text{A9})$$

Alternatively, one could calculate the residence time by averaging Eq. (A7) over the probability of first scattering $P(r_0) \simeq \exp[-(r_f - r_0)/l_{\text{sc}}]/l_{\text{sc}}$, but this would lead to similar results.

We thus find that the trapping time is of order of the crossing time, an unexpected result. Since the particle diffuses, the linear length scale traveled in this trapping time is only $l \sim (l_{\text{sc}}/r_f)^{1/2} r_f \ll r_f$. Hence the particle enters and exits the filament at about the same location, albeit a crossing time later. In terms of angular scattering, this interaction is thus akin to mirroring, as the particle will exit in a direction separated by less than $\pi/2$ from the direction of entry in the filament.

This law $\delta t_f \simeq r_f/c$ has been verified numerically, using Monte Carlo simulations of the interaction of a particle with a magnetized filament, for various coherence lengths of the magnetic field. The numerical code used has been described in detail in Ref. [52]. The results are shown in Fig. 8 below, where it is seen that the average residence time does not depend on the coherence length of the magnetic field (which characterizes the diffusion coefficient, hence the scattering length), but evolves linearly with the filament radius. Numerically, one obtains $\delta t_f \simeq 1.3r_f/c$.

3. Diffusive interaction with a sphere

The interaction with a sphere of radius r_s is quite similar to that with a filament, although the algebra is slightly more cumbersome. As before, we assume that the particle penetrates a length scale l_{sc} before starting to diffuse in the magnetized sphere, and adopt appropriate boundary conditions at radius r_s . The diffusion equation in spherical coordinates reads:

$$\partial_t g - \frac{D}{r^2} \partial_r (r^2 \partial_r g) - \frac{D}{r^2 \sin \theta} \partial_\theta (\sin \theta \partial_\theta g) - \frac{D}{r^2 \sin^2 \theta} \partial_\phi^2 g = \frac{1}{r^2 \sin \theta} \delta(r - r_0) \delta(\theta - \theta_0) \delta(\phi - \phi_0) \delta(t - t_0). \quad (\text{A10})$$

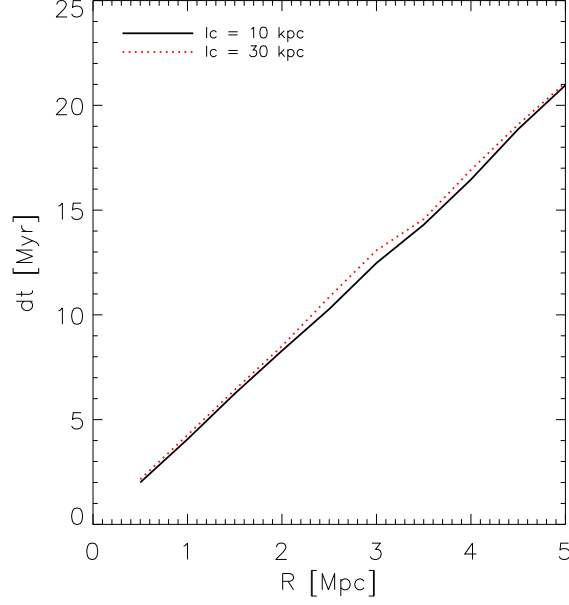


FIG. 8: Residence time in a magnetized filament embedded in a non-magnetized medium for a particle impinging on the filament with a scattering length $l_{sc} \ll r_f$, as a function of the radius of the filament. The scattering length is a function of the coherence length of the magnetic field λ , that corresponds to the modelling of Kolmogorov turbulence inside the filament, i.e. $l_{sc} \propto \lambda^{2/3}$, see Ref. [52].

Its solution is written in terms of spherical harmonics and spherical Bessel functions:

$$g(r, \theta, \phi, t; r_0, \theta_0, \phi_0, t_0) = \sum_{l=0}^{+\infty} \sum_{m=-l}^{m=+l} \sum_{s=1}^{s=+\infty} e^{-\beta_{ls}^2 \frac{D|t-t_0|}{r_s^2}} Y_{lm}(\theta, \phi) \bar{Y}_{lm}(\theta_0, \phi_0) \times j_l\left(\beta_{ls} \frac{r}{r_s}\right) j_l\left(\beta_{ls} \frac{r_0}{r_s}\right) \frac{2}{r_s^3 j_{l+1}^2(\beta_{ls})}. \quad (\text{A11})$$

The notation β_{ls} indicates the s -th zero of the spherical Bessel function j_l . As before, the probability of residence inside the spherical structure at time $t > t_0$ can be computed by integrating g over the volume:

$$P_{\text{res}}(t; t_0) = \sum_{s=1}^{s=+\infty} e^{-\beta_{0s}^2 \frac{D|t-t_0|}{r_s^2}} j_0\left(\beta_{0s} \frac{r_0}{r_s}\right) \frac{2}{\beta_{0s} j_1(\beta_{0s})}. \quad (\text{A12})$$

Here as well, $P_{\text{res}}(t \rightarrow t_0) = 1$ as it should. Finally, the residence time can be calculated by taking the limit $r_0 \rightarrow r_s(1 - l_{sc}/r_s)$ as before and expanding to first order in l_{sc}/r_s :

$$\delta t_s = \int_{t_0}^{+\infty} dt P_{\text{res}}(t; t_0) \simeq \frac{r_s}{c} \sum_{s=1}^{s=+\infty} \frac{6}{\beta_{0s}^2} = \frac{r_s}{c}. \quad (\text{A13})$$

The particle bounces on the sphere, exiting at a distance $l \sim (l_{sc}/R)^{1/2} R \ll R$ away from its point of impact.

4. Non uniform magnetic field

The above discussion has assumed that the magnetic field and the diffusion coefficient are uniform in the scattering center. If the length scale of variation of the magnetic field, $l_B = |\nabla B^2/B^2|^{-1}$ is “small enough”, the dis-

cussion becomes more intricate as the scattering length of the cosmic ray becomes itself space dependent, and meaningless if it is larger than l_B . Nevertheless, one may expect the following to occur.

If the scattering length as measured everywhere in the scattering center is larger than its size r , then the total

deflection will remain much smaller than unity. Its value will be given by an average of order $\langle rl_B/r_L^2 \rangle$, where the average is to be taken on r_L (through its spatial dependence via B) on the trajectory. This estimate assumes that the particle is deflected by $\delta\theta^2 \sim (l_B/r_L)^2$ every l_B . Its corresponds to the estimate of the above discussion if λ_B is replaced by l_B and if B is understood as the average magnetic field. The crossing time will remain unchanged, of order r/c .

If the scattering length is everywhere smaller than r , then the above results should not be modified, i.e. the particle will bounce on the scattering center with a trapping time of order r/c .

Consider now the intermediate case, for instance that

where the scattering center has a core with a magnetic field such that l_{sc} becomes smaller than the size of the core r_c , surrounded by an envelope with B such that $l_{sc} \gtrsim r$. With probability $\sim (r_c/r)^2$, the particle may cross the envelope and bounce on the core; in this case the deflection angle is of order unity and the total crossing time of order r/c . With probability $\sim 1 - (r_c/r)^2$, the particle may also cross the envelope without interacting with the core and suffer a deflection smaller than unity as calculated above; the crossing time remains the same. The typical deflection angle over many interactions of for many particles is of course given by the average of these two possibilities.

-
- [1] J. Abraham et al. (Pierre Auger), *Science* **318**, 939 (2007), arXiv:0711.2256 [astro-ph].
- [2] T. P. a. Collaboration (2007), arXiv:0712.2843 [astro-ph].
- [3] T. Stanev, P. L. Biermann, J. Lloyd-Evans, J. P. Rachen, and A. A. Watson, *Physical Review Letters* **75**, 3056 (1995), arXiv:astro-ph/9505093.
- [4] P. G. Tinyakov and I. I. Tkachev, *Soviet Journal of Experimental and Theoretical Physics Letters* **74**, 445 (2001), arXiv:astro-ph/0102476.
- [5] D. S. Gorbunov, P. G. Tinyakov, I. I. Tkachev, and S. V. Troitsky, *ArXiv Astrophysics e-prints* (2004), astro-ph/0406654.
- [6] P. G. Tinyakov and I. I. Tkachev, *Phys. Rev. D* **69**, 128301 (2004), arXiv:astro-ph/0301336.
- [7] N. W. Evans, F. Ferrer, and S. Sarkar, *Phys. Rev. D* **69**, 128302 (2004), arXiv:astro-ph/0403527.
- [8] R. U. Abbasi, T. Abu-Zayyad, J. F. Amann, G. Archbold, K. Belov, J. W. Belz, S. BenZvi, D. R. Bergman, S. A. Blake, J. H. Boyer, et al., *Astrophys. J.* **636**, 680 (2006).
- [9] Y. Uchihori, M. Nagano, M. Takeda, M. Teshima, J. Lloyd-Evans, and A. A. Watson, *Astroparticle Physics* **13**, 151 (2000), arXiv:astro-ph/9908193.
- [10] G. R. Farrar, A. A. Berlind, and D. W. Hogg, *Astrophys. J. Lett.* **642**, L89 (2006), arXiv:astro-ph/0507657.
- [11] R. U. Abbasi, T. Abu-Zayyad, J. F. Amann, G. Archbold, R. Atkins, J. A. Bellido, K. Belov, J. W. Belz, S. Y. Ben-Zvi, D. R. Bergman, et al., *Astrophys. J.* **623**, 164 (2005).
- [12] P. P. Kronberg, *Rep. Prog. Phys.* **57**, 325 (1994).
- [13] J. P. Vallee, *Fundamentals of Cosmic Physics* **19**, 1 (1997).
- [14] P. P. Kronberg, H. Lesch, and U. Hopp, *Astrophys. J.* **511**, 56 (1999).
- [15] G. T. Birk, H. Wiechen, H. Lesch, and P. P. Kronberg, *Astron. Astrophys.* **353**, 108 (2000).
- [16] S. Bertone, C. Vogt, and T. Enßlin, *Month. Not. Roy. Astron. Soc.* **370**, 319 (2006), arXiv:astro-ph/0604462.
- [17] M. J. Rees and G. Setti, *Nature (London)* **219**, 127 (1968).
- [18] S. R. Furlanetto and A. Loeb, *Astrophys. J.* **556**, 619 (2001), arXiv:astro-ph/0102076.
- [19] Gopal-Krishna and P. J. Wiita, *Astrophys. J. Lett.* **560**, L115 (2001), arXiv:astro-ph/0108117.
- [20] L. M. Widrow, *Rev. Mod. Phys.* **74**, 775 (2002).
- [21] G. Sigl, F. Miniati, and T. A. Enßlin, *Phys. Rev. D* **70**, 043007 (2004).
- [22] K. Dolag, D. Grasso, V. Springel, and I. Tkachev, *Journal of Cosmology and Astro-Particle Physics* **1**, 9 (2005), arXiv:astro-ph/0410419.
- [23] H. Takami and K. Sato, *ArXiv e-prints* **706** (2007), 0706.3666.
- [24] H. Kang, S. Das, D. Ryu, and J. Cho, *ArXiv e-prints* **706** (2007), 0706.2597.
- [25] K. Dolag, *Astronomische Nachrichten* **327**, 575 (2006), arXiv:astro-ph/0601484.
- [26] G. Medina-Tanco and T. A. Enßlin, *Astroparticle Physics* **16**, 47 (2001), arXiv:astro-ph/0011454.
- [27] P. P. Kronberg, Q. W. Dufton, H. Li, and S. A. Colgate, *Astrophys. J.* **560**, 178 (2001), arXiv:astro-ph/0106281.
- [28] L. Ferrarese and H. Ford, *Space Science Reviews* **116**, 523 (2005), arXiv:astro-ph/0411247.
- [29] E. R. Seaquist and N. Odegard, *Astrophys. J.* **369**, 320 (1991).
- [30] M. Pettini, S. A. Rix, C. C. Steidel, K. L. Adelberger, M. P. Hunt, and A. E. Shapley, *Astrophys. J.* **569**, 742 (2002), arXiv:astro-ph/0110637.
- [31] K. L. Adelberger, C. C. Steidel, A. E. Shapley, and M. Pettini, *Astrophys. J.* **584**, 45 (2003), arXiv:astro-ph/0210314.
- [32] T. M. Heckman, in *Gas and Galaxy Evolution*, edited by J. E. Hibbard, M. Rupen, and J. H. van Gorkom (2001), vol. 240 of *Astronomical Society of the Pacific Conference Series*, pp. 345–+.
- [33] A. Aguirre, L. Hernquist, J. Schaye, D. H. Weinberg, N. Katz, and J. Gardner, *Astrophys. J.* **560**, 599 (2001), arXiv:astro-ph/0006345.
- [34] R. Cen, K. Nagamine, and J. P. Ostriker, *Astrophys. J.* **635**, 86 (2005), arXiv:astro-ph/0407143.
- [35] S. Bertone, F. Stoehr, and S. D. M. White, *Month. Not. Roy. Astron. Soc.* **359**, 1201 (2005), arXiv:astro-ph/0402044.
- [36] E. Scannapieco, C. Pichon, B. Aracil, P. Petitjean, R. J. Thacker, D. Pogosyan, J. Bergeron, and H. M. P. Couchman, *MNRAS* **365**, 615 (2006), arXiv:astro-ph/0503001.
- [37] H.-P. Reuter, U. Klein, H. Lesch, R. Wielebinski, and P. P. Kronberg, *Astron. Astrophys.* **256**, 10 (1992).
- [38] F. Govoni, M. Murgia, L. Feretti, G. Giovannini, K. Dolag, and G. B. Taylor, *Astron. Astrophys.* **460**,

- 425 (2006), arXiv:astro-ph/0608433.
- [39] M. Brüggen, M. Ruszkowski, A. Simionescu, M. Hoeft, and C. Dalla Vecchia, *Astrophys. J. Lett.* **631**, L21 (2005), arXiv:astro-ph/0508231.
- [40] A. G. Doroshkevich, D. L. Tucker, R. Fong, V. Turchaninov, and H. Lin, *Month. Not. Roy. Astron. Soc.* **322**, 369 (2001).
- [41] F. Miniati, D. Ryu, H. Kang, T. W. Jones, R. Cen, and J. P. Ostriker, *Astrophys. J.* **542**, 608 (2000), arXiv:astro-ph/0005444.
- [42] H. Kang, D. Ryu, R. Cen, and D. Song, *ApJ* **620**, 21 (2005), arXiv:astro-ph/0410477.
- [43] R. M. Kulsrud, R. Cen, J. P. Ostriker, and D. Ryu, *ApJ* **480**, 481 (1997), arXiv:astro-ph/9607141.
- [44] A. Loeb and E. Waxman, *Nature* **405**, 156 (2000), arXiv:astro-ph/0003447.
- [45] F. Miniati, *MNRAS* **337**, 199 (2002), arXiv:astro-ph/0203014.
- [46] U. Keshet, E. Waxman, A. Loeb, V. Springel, and L. Hernquist, *ApJ* **585**, 128 (2003), arXiv:astro-ph/0202318.
- [47] J. Vink and J. M. Laming, *ApJ* **584**, 758 (2003), arXiv:astro-ph/0210669.
- [48] E. G. Berezhko, L. T. Ksenofontov, and H. J. Völk, *AA* **412**, L11 (2003), arXiv:astro-ph/0310862.
- [49] E. Waxman and J. Miralda-Escudé, *MNRAS* **472**, 89 (1996).
- [50] K. Greisen, *Phys. Rev. Lett.* **16**, 748 (1966).
- [51] G. T. Zatsepin and V. A. Kuzmin, *JETP Lett.* **4**, 78 (1966).
- [52] K. Kotera and M. Lemoine (2007), arXiv:0706.1891 [astro-ph].
- [53] R. Teyssier, *A&A* **385**, 337 (2002).
- [54] J. Alvarez-Muñiz, R. Engel, and T. Stanev, *Astrophys. J.* **572**, 185 (2002), arXiv:astro-ph/0112227.
- [55] H. Takami and K. Sato, *ArXiv e-prints* **711** (2007), 0711.2386.
- [56] E. Waxman, *Physical Review Letters* **75**, 386 (1995), arXiv:astro-ph/9505082.
- [57] M. Lemoine, G. Sigl, A. Olinto, and D. N. Schramm, *ApJ* **486**, L115 (1997).
- [58] E. Waxman, in *Physics and Astrophysics of Ultra-High-Energy Cosmic Rays*, edited by M. Lemoine and G. Sigl (2001), vol. 576 of *Lecture Notes in Physics*, Berlin Springer Verlag, pp. 122–+.
- [59] G. Sigl, M. Lemoine, and P. Biermann, *Astropart. Phys.* **10**, 141 (1999), astro-ph/9806283.
- [60] R. Aloisio and V. Berezhinsky, *ApJ* **612**, 900 (2004).
- [61] M. Lemoine, *Phys. Rev. D* **71**, 083007 (2005).
- [62] R. Aloisio and V. Berezhinsky, *ApJ* **625**, 249 (2005).
- [63] V. Berezhinsky and A. Gazizov, *ApJ* **643**, 8 (2006).
- [64] J.-P. Bouchaud and A. Georges, *Phys. Rep.* **195**, 127 (1990).
- [65] R. C. Ball, S. Havlin, and G. H. Weiss, *Journal of Physics A Mathematical General* **20**, 4055 (1987).
- [66] C. A. Norman, D. B. Melrose, and A. Achterberg, *Astrophys. J.* **454**, 60 (1995).
- [67] F. Casse, M. Lemoine, and G. Pelletier, *Phys. Rev. D* **65**, 023002 (2002).
- [68] D. Gorbunov, P. Tinyakov, I. Tkachev, and S. Troitsky (2007), arXiv:0711.4060 [astro-ph].
- [69] E. Waxman, K. B. Fisher, and T. Piran, *Astrophys. J.* **483**, 1 (1997), arXiv:astro-ph/9604005.
- [70] V. Berezhinsky, A. Gazizov, and S. Grigorieva, *Phys. Rev. D* **74**, 043005 (2006), arXiv:hep-ph/0204357.
- [71] J. Giacalone and J. R. Jokipii, *Astrophys. J.* **520**, 204 (1999).
- [72] J. Candia and E. Roulet, *JCAP* **0410**, 007 (2004).
- [73] <http://www-akeno.icrr.u-tokyo.ac.jp/AGASA/>
- [74] <http://www.augernorth.org>